Received: 1 June 2022 | Revised: 20 July 2022 | Accepted: 1 August 2022

DOI: 10.1002/eom2.12281

EcoMat FUNCTIONAL MATERIALS FOR GREEN ENERGY AND ENVIRONMENT WILEY

REVIEW

Recent advances of non-fullerene organic solar cells: From materials and morphology to devices and applications

Ying Zhang | **Yongwen Lang** | **Gang Li**

The Department of Electronic and Information Engineering, Research Institute for Smart Energy (RISE), The Hong Kong Polytechnic University, Hong Kong, China

Correspondence
Gang Li, The Department of Electronic and Information Engineering, Research Institute for Smart Energy (RISE), The Hong Kong Polytechnic University, Hong Kong 999077, China.
Email: gang.w.li@polyu.edu.hk

Funding information
Guangdong-Hong Kong-Macao Joint Laboratory for Photonic-Thermal-Electrical Energy Materials and Devices, Grant/Award Number: 2019B121205001; Hong Kong Polytechnic University; Sir Sze-yuen Chung Endowed Professorship Fund, Grant/Award Number: 8-8480; Shenzhen Science and Technology Innovation Commission, Grant/Award Number: JCYJ 20200109105003940; Research Grants Council of Hong Kong, Grant/Award Numbers: C5037-18G, 15221320

Abstract

The innovation of non-fullerene acceptors (NFAs) enables the rapid progress of organic solar cells (OSCs) in power conversion efficiencies to over 19%, endowing OSCs with great potential toward real-world application. In this critical review, we outline the recent advances of NFA-based OSCs - from ITIC- to Y6-family, to exemplify the structure–performance correlations, and cover from material chemistry to nanomorphology controlling. In addition, we point out the possible degradation mechanisms behind the NFA-based devices and strategies for mitigating the stability issues. With OSC efficiencies approaching 20% benchmark, increasing attention has been built-up toward the technology's applications. Therefore, we describe the opportunities and challenges in the promising applications, mainly on semitransparent and flexible OSCs for commercial photovoltaics. Finally, we provide a summary and perspective to point out the primary challenges the OSC technology is facing toward commercialization.

KEYWORDS

applications, material chemistry, morphology, non-fullerene organic solar cells, stability

1 | INTRODUCTION

Organic solar cells (OSCs) are attracting the increasing attention of the research community as a promising next-generation photovoltaic technology (PV) because of their competitive advantages such as lightweight, semitransparency, together with mechanical flexibility, and roll-to-roll production.[1–5] The OSCs are typically based on organic semiconductors that constitute π-conjugated carbon-based backbones with alternating C—C single bond and C═C double bond, where electrons can be readily delocalized along with conjugated skeletons on P_z orbitals.[6] Notably, the most significant variation between organic and inorganic semiconductors is that the dielectric constant (ε) of organic material is relatively low (2–4), suggesting strong binding energy ($0.3 \sim 1$ eV) between electron and hole (so-called bounded Frenkel excitons rather than free carriers).[7] Historically, the advent of OSCs dates back to 1986, when Tang firstly introduced a two-component OSC in the layer-by-layer configuration fabricated by vacuum evaporation to generate current by utilizing the energy offsets between an electron donor (D) and electron acceptor (A) material as a driving force to overcome the excitons' binding energy

to dissociate them into carriers.[8] However, the limited D: A interfacial areas in such planar heterojunction results in low exciton dissociation efficiency and thus low device photocurrent. In 1992, Heeger and co-workers demonstrated ultrafast electron transfer from polymer to C60,[9] and in 1995, Heeger and Wudl proposed a bulk heterojunction (BHJ) structure by blending D and A in one solution for blend casting, contributing to significant improvements in photocurrent.[10] By constructing more D/A interfacial areas, the pioneering BHJ architecture subsequently has been dominant in the following decades and made the most contributions to pushing the efficiency forward in OSCs. Single-junction BHJ OSCs have experienced massive progress in the power conversion efficiencies (PCEs) of 18%–19%.[11–13] Such rapid development of OSCs is tightly associated with the innovation of material science, morphology control, and device physics.

Generally, material science and morphology optimization are two kernels pushing the OSCs efficiency toward future commercialization.[14] Three key parameters determine the efficiency of an OSC: $PCE = J_{SC} \times V_{OC} \times FF/P_{in}$, where J_{SC} is short circuit current density, V_{OC} is open-circuit voltage, FF is fill factor, and P_{in} is the incident light power intensity. Aiming at improving PCEs of OSCs, the three parameters above should be increased, and material science plays a pivotal role in determining how far these parameters can reach. Specifically, J_{SC} is closely linked to the optical bandgap (E_g) of material, which determines the absorption range of the solar spectrum.[15,16] V_{OC} is determined by the energy difference between the highest occupied molecular orbital (HOMO) of donor material and the lowest unoccupied molecular orbital (LUMO) of acceptor material.[17–19] FF is the most complicated part because this parameter is affected by many factors, such as carrier mobility, active layer morphology, and interfacial and bulk charge recombination. There is evidence that the reasonably fine-tuned nanomorphology and the balanced carrier mobility of the active layer can contribute to the increased FF of OSCs.[20–22] There is thus an urgent need for designing and synthesizing donors and acceptors, focusing on adjusting their respective E_g with complementary absorption, well-matched energy levels, and adequately compatible nanostructure in the active layer.[23,24] At the infant stage of OSCs (i.e., the fullerene era), numerous research efforts were devoted to the development of polymer donors or small-molecular donors due to the limited chemical modification of fullerene derivatives (such as [6,6]-phenyl-C61 butyric acid methyl ester [$PC_{60}BM$] or [6,6]-phenyl-C71 butyric acid methyl ester [$PC_{70}BM$]).[23] Versatile donor materials were successively developed for fullerenes, involving polymer donors of polythiophene derivative (P3HT) and D-A types (such as PTB-series,[25] PffBT4T-2OD,[26] and small molecular donors), (e.g., DRCN4T-DRCN9T[27] and BTR[28]), triggering continuously improved performances when blended with fullerene derivatives. Fullerene-based OSCs, however, suffer from low photocurrent and photovoltage mainly because of the intrinsically poor absorption ability and limited energy-level tunability of fullerenes, respectively.[29,30] In addition, fullerenes tend to excessively aggregate upon thermal stresses, which leads to poor thermal stability.[31] This situation has changed until the boom of non-fullerene acceptors (NFAs). Compared to fullerenes derivatives, the tunable E_g and energy levels in NFAs through molecular modification strategies can provide more access to devices with a high V_{OC} and high J_{SC} that are otherwise not possible in fullerene-based OSCs.[32,33] For instance, downshifting HOMO of donor and/or upshifting LUMO of acceptor benefit the photovoltage and narrowing E_g of materials can increase photocurrent, respectively.[34,35]

Besides the intrinsically optical and electrical properties, it is well acknowledged that active layer morphology plays a crucial role in governing the device performances by affecting the charge dynamics.[36] Since researchers in 2005 underscored the importance of BHJ morphology controlling in significantly impacting the photovoltaic parameters, the influence of BHJ morphology on the photovoltaic parameters has been widely elucidated.[37,38] There typically exist several possible scenarios in a BHJ structure: ordered crystallites, relatively pure donor and acceptor domains, and mixed amorphous domains, which will influence the charge transport and charge separation, respectively.[39] Therefore, morphology tuning provides an opportunity to enable performance improvements (especially J_{SC} and FF).[40] Nonetheless, challenges for BHJ morphology optimization are waiting to be tackled. An ideal BHJ morphology that can balance the charge separation and charge transport is key to achieving high-efficiency OSCs. Many factors, such as the thermodynamic miscibility and film formation kinetics of materials, should be considered together to form the final morphology including the mixed and crystalline domains.[41,42] In addition, various morphology optimization strategies developed initially for fullerene-based OSCs are found effective to tune the NFAs-based OSCs. The chemically evolved structures of NFAs in OSCs also imply new morphology optimization mechanisms, which could be fundamentally different from those in fullerene-based OSCs, and thereby it is strongly desirable to find novel active layer engineering protocols beyond the traditional ones.

Overall, an in-depth understanding of material science and morphology control are two key contributions that provide fundamental structure-performance correlations in order to develop more efficient NFA-OSCs. In

the historical development of NFAs, push-pull-type small molecular acceptors (SMAs) opened up two main phases from ITIC-families to Y-series.[43,44] To date, Y-series NFAs have promoted the efficiencies of OSCs over 19%.[12] For this reason, summarizing the critical achievements in Y6-type NFAs by distinguishing the key aspects of material design concept and blend morphology control in comparison with ITIC-likes and trying to give the reason why Y6 performs well is necessary. Moreover, it is a timely review of the latest progress in sequential-deposited, scalable, transparent, and flexible organic photovoltaic (OPV) technology. Generally, this review has covered the comprehensive topic from materials and morphology to devices and applications, providing a general guideline for the further evolution of Y-series, which is less systematically touched by other reviews on Y6-like NFAs.[45,46] Based on this, this review will provide an overview of the most recent progress in material chemistry by exemplifying their structure–property correlation, with a particular focus on the state-of-the-art NFAs mainly evolutionary from ITIC-families to Y6-likes, hoping to infer a guideline, for example, further advancement of properties of Y-series, to facilitate the further breakthrough in efficiencies. Second, we highlight the recent insights into morphology optimization strategies by rationally tuning small molecules' aggregation behaviors and characterization tools. Third, we shed light on the degradation mechanisms behind the devices to give an indicative hint for optimizing device stability by guiding materials design and morphology control. Then, we briefly describe the opportunities and challenges in the promising applications, mainly on semitransparent and flexible OSC. Finally, we give a summary and perspective on the future development directions of OSCs.

2 | MATERIAL CHEMISTRY EVOLUTION OF NFAS FROM ITIC TO Y6

Undoubtedly, the concerted efforts in materials synthesis of donors and acceptors will undoubtedly promote the development of OSCs, where the synthesis strategies mainly include core engineering, side-chain engineering, and end-group.[47] Since many excellent reviews have given a specialized summarization of synthetic efforts in materials design,[48,49] in this section, we emphasize the major differences in chemical structure-device performance relationships between ITIC-type and Y6-type acceptors. The representative chemical structures of donors and acceptors are shown in Figure 1A,B, respectively.

In 2015, a turning point, the star small molecular acceptor (SMA)-based NFA named ITIC emerged with electron push and pulling effects induced by alternating electron-donating and electron-accepting units (A-D-A). Since then, ITIC and its likes based on A-D-A alignment have arisen unparalleled interests in the OPV community.[43,50] Mindful that ITIC is so distinct compared to fullerenes, the molecular geometry is optimized as an indacenodithienothiophene (IDTT) electron-donating core attached by largely branched side chains and two dicyanomethylene-1-indanone (IC) electron-withdrawing end groups. Such chemical structure introduces three distinguished properties and perspective possibilities for devices: (1) push-pull effects can induce a strong intramolecular interaction that possibly affords a reasonably narrow bandgap (E_g) with broader absorption to the NIR region of the solar spectrum; (2) the D-A interaction leads to a strong intramolecular charge transfer (ICT) effect, which effectively reduces the difference between HOMO and LUMO energy levels of the acceptor, thus leading to greater oscillator strength with strong absorption coefficients. Thus, the A-D-A type NFAs can show high photocurrent, almost doubling that of fullerenes and perylene diimide (PDI)-based SMAs; (3) unlike isotropic charge transport in fullerenes, this geometry will facilitate intermolecular charge transport pathway via adjacent acceptor molecules and/or charge transfer to the donor through end-group π–π stacking when blended with the donor.[20,51] Additionally, this rigid molecular conformation can maintain good molecular planarity and preferably crystallize in the solid state, thereby ensuring high electron mobility in both films and devices.[33] Prodigious amounts of synthetic attempts are consequently made to carefully modify ITIC chemically, focusing on modulating ICT effects to tune the absorption spectra and energy levels in order to improve photovoltaic parameters.[3,52] For instance, Hou et al. substituted the phenyl-fused indanone in the end-capping units of the ITIC molecule with a more electron-donating thiophene group (ITCC), which leads to a weaker ICT effect with the strong electron-donating core, resulting in elevated LUMO energy level. As a result, the OSCs based on PBDB-T: ITCC delivered a higher V_{OC} value of over 1 V. However, the J_{SC} was not high due to the blue-shifted absorption compared with ITIC.[53] There is, therefore, a trade-off between high current and high photovoltage when attempting to rationally design novel molecules for OSC devices.[54] Apart from end group modulation, the choice of extended conjugation is critical to the E_g modulation and thus absorption spectra of IDT-based SMAs. For example, the E_g of ITIC can be reduced by extending the seven-ring core to nine-ring fused cores (INIC) from 1.70 to 1.57 eV, which extended the absorption edge to 900 nm.[55] It is noticed that the side-chain modification will control the intermolecular packing and the aggregation of IDT-based SMAs in solid films with minor

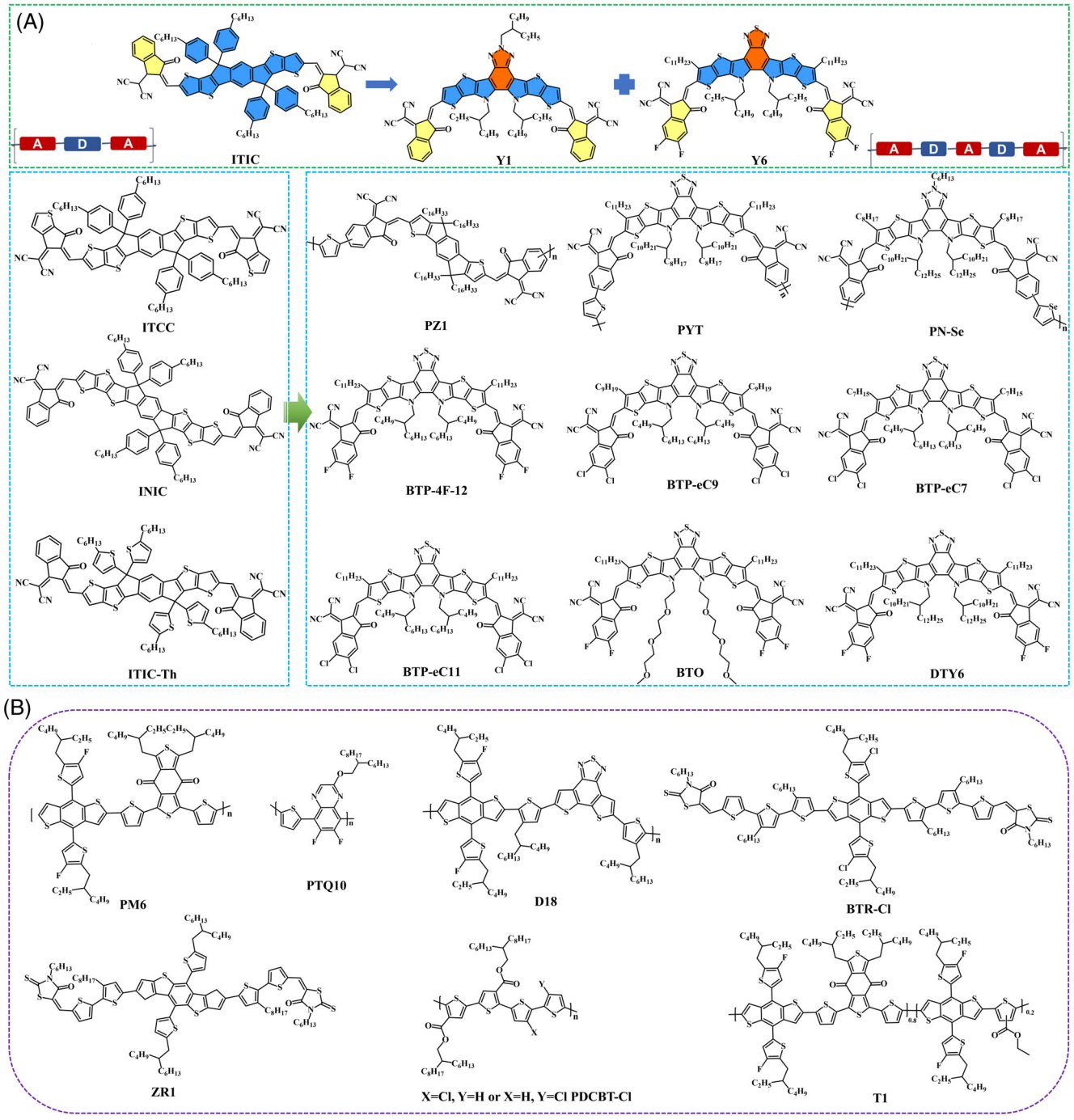

FIGURE 1 (A) The chemical structures of representative non-fullerene acceptors and (B) donors involved in this review

changes in energy levels. Zhan et al. demonstrated that thienyl side-chains substituents (ITIC-Th) displayed enhanced intermolecular interaction due to sulfur–sulfur non-covalent interactions compared to alkyl phenyl side chains (ITIC), leading to higher electron mobility (6.1×10^{-4} cm^2 V^{-1} s^{-1}).[56] With the integrated contributions of chemical modifications and material screening out, record efficiencies of OSCs devices involving ITIC-families lie around 13%–14% PCEs.[57,58]

This efficiency plateau has not been broken through until early 2019 when another star SMA-Y series were innovated as A-D-A′-D-A type following the molecular design concept (push–pull effects) in ITIC, first Y1 and then Y6 with a PCE of exceeding 15% in single-junction OSC history.[44,59] To be specific, this bent-shaped molecular motif is composed of the same end-capping groups with ITIC and a new electron-deficient-core dithienothiophen [3,2-b]-pyrrolobenzothiadiazole (TPBT) via

introducing an electron-deficient unit benzo[c][1,2,5] thiadiazole (BT) moiety. The specific structural features are highlighted herein. First, compared with A-D-A-type SMAs, the insertion of an electron-negative core in Y-series SMAs allows for more pairs of D–A interactions and enables stronger ICT effects, leading to their narrower E_g; for example, the stronger absorption extended to 930 nm with a smaller optical E_g of 1.33 eV can be achieved in Y6 with BT unit as the core. The resultant device showed a high J_{SC} value of over 25 mA cm^{-2} when matching with polymer donor PM6.[60] More excitingly, meantime, the deep HOMO energy level with small energy loss (E_{loss}) can be obtained in this type of electron acceptor, which was previously demonstrated in Y1 and Y2 molecules with benzotriazole as electron-deficient core, giving a lower E_{loss} value (0.57 V vs. 0.7 eV in ITIC) due to the stronger electroluminescent quantum efficiency (EQE_{EL}) of Y1. Second, the sp^3-hybridized carbon atoms of IDTT core are replaced by sp^2-hybridized nitrogen of pyrrole rings, which enhances the conjugation and charge mobility, reduces E_g, and broadens absorption.[59] Third, and more prominent, the bulky aromatic side chains are alternatively changed to alkyl side chains, which will reduce the steric effects and induce the preferably special inter-chain packing between the core and end-group, or two cores (coexistence of J-type and H-type aggregates). This will benefit high electron transport in films that contribute to the enhancement of the ultrafast hole transfer and multiple charge transport pathways in devices. Such a molecular packing strongly contrasts with the ITIC analogs—bulky aromatic side chains lead to the strong steric effects on the fused cores. They will limit the intermolecular interaction between cores, which predominantly contains J-type aggregates (via terminal moieties π–π packing) with very few cases like COi8FOIC molecule featuring both J-type and H-type aggreagtions.[52,61] The different molecular packing modes of ITIC-type acceptors and Y6-type acceptors can be validated via analyzing their single-crystal structures, which will be discussed in the following morphology part. Moreover, the solubility and molecular packing of NFAs can be regulated by modifying the side chains attached to the conjugated skeletons.[60] Generally, the variation of electron-deficient cores above has major effects on the energy levels and molecular packing.[62] Side-chain engineering is more powerful for controlling intermolecular interaction.[63] It seems that the highlight of Y-series NFAs is the small E_g while maintaining the deep energy levels that can match well with the commonly used polymer donors, like BDT-based polymer donor (e.g., PBDB-T and PM6),[64,65] D18[66] with the temperature-dependent aggregation feature, PTQ10,[67] liquid crystal small molecular donor (BTR-Cl),[68] that are previously well applicable for ITIC-families.

SM-NFAs discussed above can provide an exciting opportunity to promote the development of all-polymer solar cells (all-PSCs). All-PSCs have great potential to improve light and thermal stability.[69] Still, the most representative electron-deficient imide-based polymer acceptor (like N2200) suffers a low absorption coefficient (0.3×10^5 cm^{-1} at 700 nm) and large-domain nanomorphology, resulting in low photocurrent and FF and the limited efficiency of ~11% with a minor further breakthrough in N2200-based all-PSCs.[70,71] To improve long-wavelength absorption capability is a crucial factor in enhancing PCEs of all-PSCs. Direct polymerization of highly efficient SMAs with narrow bandgaps can potentially achieve this goal; that is, distinct merits (including narrow bandgap, strong absorption, low energy loss, and appropriate energetic levels) of SMAs segments are inherited by their corresponding polymerized SMAs (PSMAs) while possessing the advantages of thermal stability as well as good mechanical flexibility.[72] In 2017, the success of polymerized SMAs strategy was firstly demonstrated by Zhang et al. through polymerizing an SMA IDIC to achieve a PSMA (PZ1).[73] As expected, the obtained PZ1 showed a red-shifted absorption in films with a medium E_g of 1.55 eV and better thermal stability in comparison with IDIC. With PBDB-T as the donor, the PZ1-based all-PSCs gained a high J_{SC} of 16.05 mA cm^{-2}, better than N2200-based devices. Likewise, the polymerization of ITIC-series triggered efforts to synthesize PSMAs with Y6-series as the central building block by taking the most advantage of their broader absorption and superior molecular packing. Jia et al. reported PJ1 that shows a narrow E_g of ~1.4 eV and a high extinction absorption of ~1.39×10^5 cm^{-1}, and PJ1-based device displayed a high PCE of 14.4% with a high J_{SC} of over 20 mA cm^{-2}, where PBDB-T is the donor.[74] They also found that the device performances, mainly J_{SC}, tend to depend on the molecular weights of PSMAs, which is explained by the fact that the high weights of PSMAs will result in the red-shifted absorption and slightly higher extinction coefficient. This molecular weight-sensitive performance is similarly observed in another PSMA - PYT with Y5-C20 as the building block developed by Min's group,[75] wherein increasing the molecular weight of PYT will slightly enhance the absorption coefficients. Consequently, with the synergetic efforts in polymer design, morphology control, and device optimization, all-PSCs have reached excellent PCEs up to 16%–17%,[76–79] gradually closing the gap with the SMAs-based OSCs. From these studies, one can tell that such PSMAs strategy is impactful in achieving high photocurrents approaching 25 mA cm^{-2} for the best example (PBDB-T: PN-Se)[76]; however, one fundamental pain point of all-PSCs, including both NDI-based copolymer and PSMAs, is their low FFs around 70%–72%, which

is inherently correlated with the nanomorphology and charge transport properties of blend films,[80,81] requiring scientific attention and fundamental understanding from the comprehensive perspectives of molecular design, material matching, and morphological properties.

One thing to notice is that the so-called PSMAs are typically not real polymers, as the repeating units' numbers are around 10, probably more appropriate to be viewed between polymer and oligomer. Oligomers are much less studied in OSC field so far, but may have unique add-on benefits to the field, considering their well-defined molecular structure, good processability, solubility, and high PL quantum efficiency, and so forth.[27] In fact, we recently found that the oligomers as the third components are more compatible with the host SMA in the ternary blend and will more readily inhibit the strong aggregation of SMA domains.[82] As a result, the aggregation-caused emission quenching effect of SMA can be greatly reduced, leading to the improvement of (EQE_{EL}) and the minimized non-radiative energy loss. Therefore, the novel device physics in this type of oligomers should arise more central research attention.

One should note that, besides photovoltaic properties, it is inevitably imperative to develop reproducible and cost-effective photovoltaic materials from the perspective of industrial commercialization of OSCs.[83] For example, the high-performance conjugated polymer donors, such as PM6 and PM7, typically suffer from severe batch-to-batch variations due to the uncontrollable fluctuation of molecular weights. To solve this problem, Duan's group developed a random molecular geometry by employing a simple building block cyanothiophene (CT) to construct a high-performance donor polymer named PBCT-2F. The polymer not only showed a high efficiency of over 17%, but also exhibited low sensitivity to a wide molecular weight range and thus has less batch-to-batch variations.[84] On the other hand, the widely used polymer donors, which are predominant by BDT and benzo-[1,2c:4,5-c']dithiophene-4,8-dione (BDD) backbones, typically require multiple synthesis steps and rigid purification processes, thus suffering from high production cost and difficult up-scaling production.[85] The polythiophene (PT)-based conjugated polymer donors are preferably developed due to their simple molecular structures recently and low cost. To date, the PT-based OSCs have surpassed 17% PCEs.[86]

3 | MOST RECENT ADVANCES IN MORPHOLOGY OPTIMIZATION AND CHARACTERIZATION

Refining the BHJ morphology of the OSC active layer is critical in improving the photovoltaic performances of devices.[87,88] The fundamental morphological parameters at multiple length scales, including molecular packing and orientation, coherence length, aggregation and phase separation, and domain purity/domain size, can depend strongly on various factors, as highlighted in three aspects, that is, the properties of donor and acceptor materials, the solubility of the material in solvents, the miscibility between donor and acceptor.[89–91] The dominant BHJ structure poses rigorous challenges to the morphology controlling due to the complex interactions between donor and acceptor during the film formation process, where phase separation and crystallization will always be challenging to balance.[92] The empirically used optimization strategies by trial and error, such as solvent/additive engineering, thermal annealing, and vapor annealing, have been demonstrated to mediate the phase separation of the active layer.[37,38,93–95] It is noteworthy that these morphological parameters are not independently manipulated, requiring comprehensive consideration for synergistic optimization of devices with an in-depth understanding of manipulation methods as a prerequisite.[96] Moreover, the morphology of OSC requires an understanding at many length scales and the fundamental structure–performance correlation coupled with multi-scale morphology characterization techniques,[97] as shown in Figure 2. Therefore, in the following, we underline the critical factors (molecular structure and thermodynamic interaction) that will exert influences on morphological properties and exemplify the morphological refining strategies that can provide insight into understanding the mechanisms by which it affects device performances.

At the nanoscale, it is well established that molecular packing, which is strongly molecular configuration dependent, can directly influence the charge transport and final performances in devices.[98,99] Prior to investigating the bulk morphology of Y-series-based OSCs, it is of major interest to first reveal the local morphology of neat NFAs films (ITIC and Y-series here) in a predictive approach to their single-crystal structures, which has been employed widely.[100–103] Yip et al. dissected a visualized molecular stacking of Y6 via crystallographic analysis.[104] They found that, in addition to marginal π–π stacking (pairs 1 and 2), the unusual face-to-face π-core interaction is allowed by benzo[2,1,3]thiadiazole sulfur–nitrogen interactions (pair 3), as illustrated in Figure 3A, which is the primary origin of three dimensional (3D) network charge transport pathways formation. The molecular structure will benefit the outstanding charge generation and transport properties and the device efficiency relative to ITIC-type acceptors. In combination with molecular dynamics (MD) simulations, it was found that the molecular packing modes (coexistence of π–π

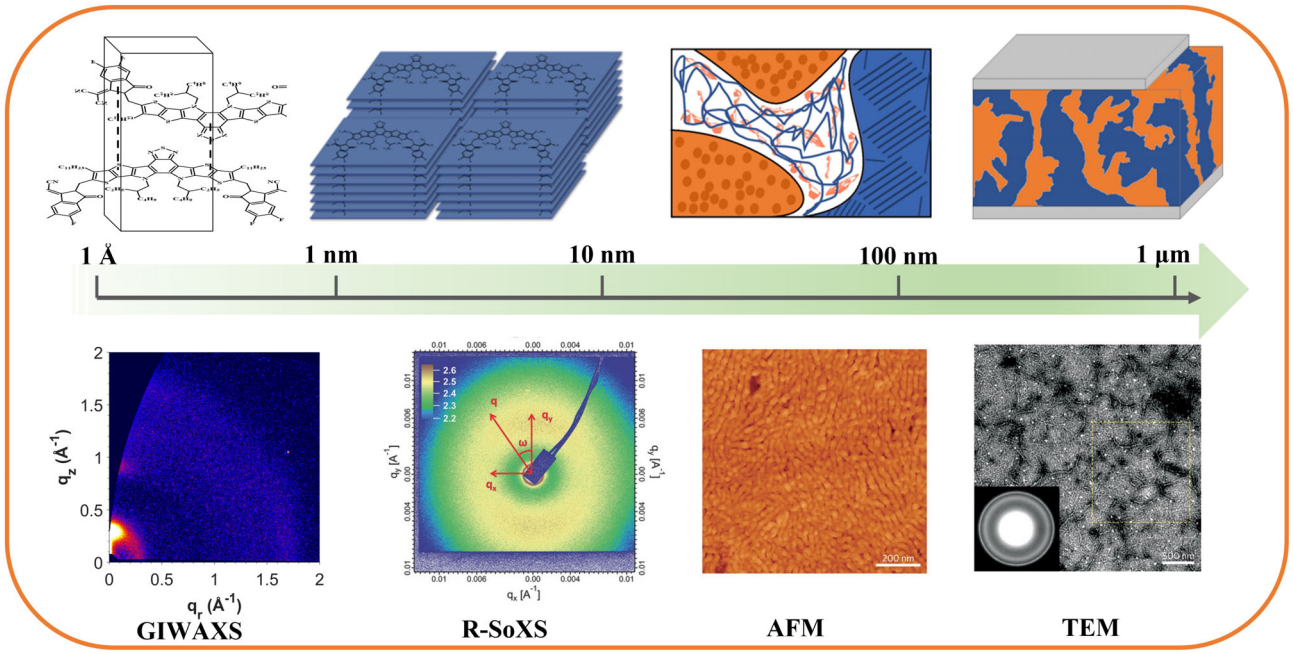

FIGURE 2 The sketch map of morphology evolution and characterizations at different length scales in organic solar cells. Reproduced with permission: Copyright 2012, Nature Publishing Group.[1] Reproduced with permission: Copyright 2017, Wiley-VCH[98]

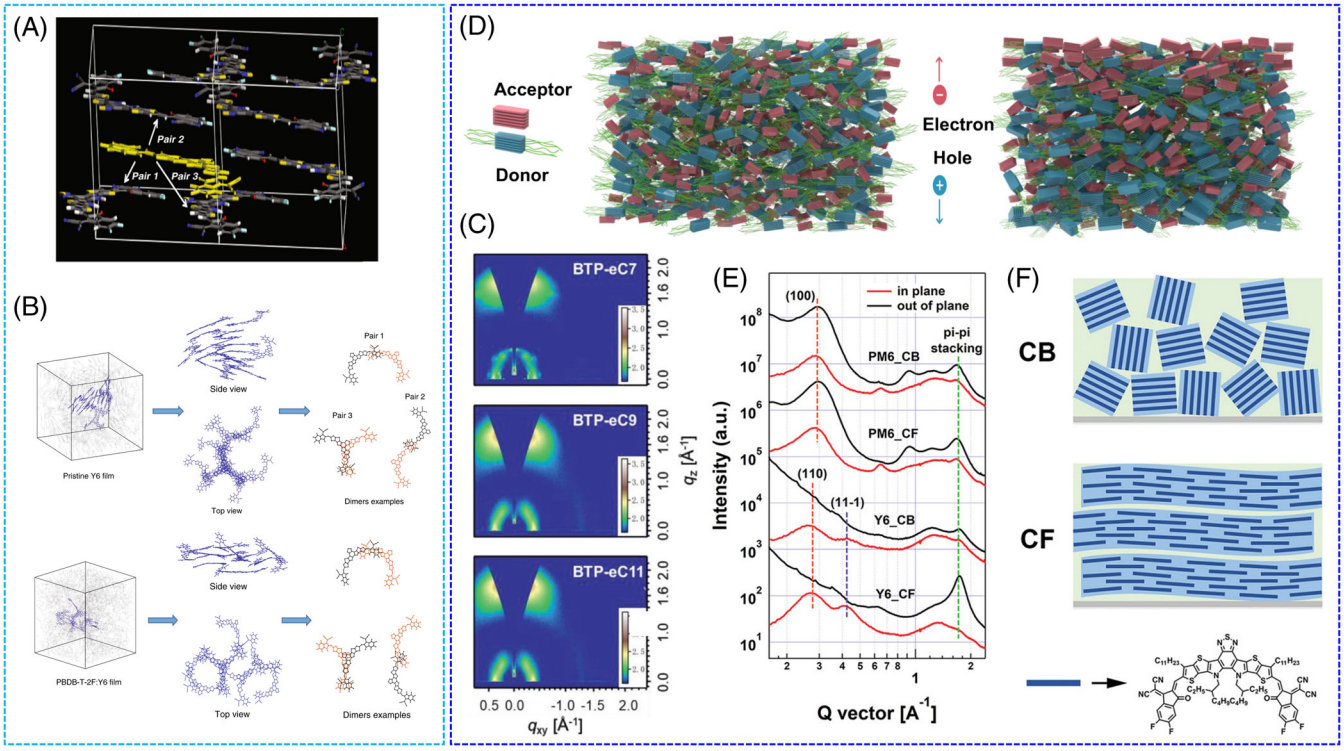

FIGURE 3 (A) Molecular pairs in the Y6 single crystal. (B) Illustration of the molecular-dynamics simulations results for the packing in b the pristine Y6 and PBDB-T-2F:Y6 films. Reproduced with permission: Copyright 2020, Springer Nature.[104] (C) 2D GIWAXS patterns of the non-fullerene acceptors films. Reproduced with permission: Copyright 2020, Wiley-VCH.[106] (D) The optimal BHJ film and the optimal G-BHJ film along the vertical direction. Reproduced with permission: Copyright 2021, Springer Nature.[92] (E) Scattering profiles for pure films of PM6 and Y6 processed with chloroform (CF) and chlorobenzene (CB) and (F) the corresponding arrangement sketch map of molecules in films processed by CB and CF. Reproduced with permission: Copyright 2020, Wiley-VCH[101]

interactions from H aggregations of cores and J aggregations of end groups) will not be altered by casting pristine Y6 thin film or the blend films with PM6 donor, as shown in Figure 3B. One can safely clarify that, when blended with polymer donor (like PM6) that serves as scaffolds to confine the crystallization of SMAs, Y6-type SMAs show a stronger self-aggregation tendency in BHJ films relative to ITIC-types.[12] Due to the solution processing characteristics in OSCs, the intrinsic solubility of materials (solvent–molecule affinities) is a critical reason that influences the film drying dynamics and molecular crystallinity of polymer-SMA system in solid state and eventual performances, especially in Y6-based systems, triggering efforts to mainly manipulate the aggregation of Y6, for example, via altering solubility and pursue a wide processing window in both halogenated and non-halogenated solvents.

On one side, many groups devoted synthetic efforts to alkyl side chain modifications of Y6 to refine its excessive aggregation for this purpose. For example, Hou et al. changed the alkyl chains on the pyrrole ring from 2-ethylhexyl on Y6 to 2-butyloctyl (BTP-4F-12), resulting in better solubility while retaining tighter lamellar stacking and better charge transport.[105] Benefiting from the superior processability, the device based on PBDB-TF: BTP-4F-12 achieved an extraordinary PCE of 16.4%. More importantly, with eco-friendly processing solvents, tetrahydrofuran (THF) and *o*-xylene (XY), the optimal devices delivered excellent PCEs of 16.1% and 15.3%, respectively, with a polymer T1 as the donor due to its better solubility than PM6. Later, the same group made another successful attempt to synthesize a series of novel molecules by subtly shortening the length of side chains in Y6 attached to the β position of the thiophene unit.[106] In this case, different lengths of alkyl chains could give rise to the tuned solubility and diverse molecular packings, as shown in two-dimensional grazing-incidence wide-angle X-ray scattering (2D-GIWAXS) of Figure 3C. In particular, the obtained BTP-eC9 molecule showed slightly inferior but reasonable solubility, leading to enhanced molecular packing in the solid state, giving a record PCE of 17.8% with an excellent FF of 81.1%. Further decreasing the length of alkyl chains to BTP-eC7 will lead to very poor solubility and thus undesirable excessive phase domains. As a result, the PM6:BTP-eC7 device gave the lowest device performance. Besides molecular engineering, recent studies have implied that the ternary strategy by adding the third component into the binary blend can feasibly achieve this solubility tuning goal. Li et al. designed and synthesized a Y6 derivative SMA (BTO) as a guest molecule to incorporate into PM6:Y6 OSC for constructing ternary OSCs.[107] The enhanced solubility of Y6 in both CF and CB along with the molecular packing of mixed acceptors after the addition of BTO enabled a high PCE of 16.59% in the optimal ternary device processed by green solvent paraxylene (PX), outperforming the corresponding binary devices (a PCE of 11.5%), and demonstrating the merits of the increased solubility strategy in the performance improvement. Based on the investigations above, it seems that the precisely suitable solubility of NFAs is a pronounced factor that governs the processability, crystalline morphology, carrier transport, and thus J_{SC} and FF.

On the other hand, thermodynamic interaction (e.g., miscibility) between donor and acceptor materials strongly affects the final morphology (i.e., nanoscale phase separation) and can provide a better understanding of how to pair an efficient donor–acceptor mixture and refine film morphology.[108,109] For instance, materials with high miscibility induce small domains in blend film, while immiscible materials can drive large domains and thus phase separation at a larger scale.[110] It is well understood that thermodynamic miscibility is inextricably intertwined with molecular structures.[24] For example, the miscibility between NFAs (like Y-type) and high-efficiency polymer donors is not a big problem due to their similar building blocks, in which the long-chain feature of conjugated polymer tends to self-aggregate to form entangled fibril structure, around which the SM-NFAs would be more readily intermixed and arranged.[12,51] The miscibility of components can be directly assessed by the Flory–Huggins interaction parameter χ, which can be experimentally determined by several methods, such as the Hansen solubility parameters, the melting point depression method and measuring surface energy (γ).[109] Among them, the most feasible/convenient way is to use the surface energy to determine the χ, following empirical equation: $\chi_{12} = k\left(\sqrt{\gamma_1} - \sqrt{\gamma_2}\right)^2$, where k is a positive constant, γ_1 and γ_2 are the surface energies of corresponding neat films and can be experimentally obtained by measuring contact angles of thin films in many OSCs studies.[111,112] To simplify, the small χ_{12} indicates the good intermixing between two molecules. Ye et al. reported that OSCs based on a novel polythiophene (PT) donor named PDCBT-Cl paired with a series of NFAs show varied device performances.[113] They subsequently investigated the underlying mechanisms from the thermodynamic point of view. The calculated χ_{12} values of PDCBT-Cl: ITIC-Th1 and PDCBT-Cl:Y6 blends are 0.14 and 0.05, respectively. Finally, the PDCBT-Cl:ITIC-Th1 system showed the best PCE of over 12%, benefiting from their proper miscibility. PDCBT-Cl:Y6, though, delivered an inferior efficiency of 0.5% due to their hyper-intermixing amorphous phases without fundamental D/A phase separation. More importantly, the thermodynamic properties can take an essential role in guiding the processing

procedure, thus enabling the way to highly efficient OSCs. Ade and coworkers elucidated that D18:Y6 OSC exhibited optimal performances under solvent vapor annealing (SVA) conditions rather than thermal annealing treatment.[114] Thermodynamic characterization revealed that the D18:Y6 blend could achieve the near the percolation threshold in mixed region at room temperature without the need for heating as a robust driving force for phase separation; thus, the mild SVA can more readily introduce the proper phase separation, resulting in a best-performing PCE of 17.31% upon SVA processing. Notedly, the critical issue of ternary OSC strategy concerning rational third component selection can be mitigated with the thermodynamic miscibility tuning in mind.[115] For example, the majority of record ternary OSCs are realized in one donor and two acceptors (D:A_1:A_2) configurations, wherein two miscible acceptors often form tighter molecular packing continuous acceptor domains, which is beneficial for charge transport and charge recombination depression.[11,69,116,117]

To optimize the morphological properties above, the most recent and promising strategies for morphology tuning should be highlighted. Besides the traditional morphology optimization strategies empirically learned from fullerene-based devices, exploring more specific NFA-oriented morphology optimization methods is crucial for further improvement of OSC. Hou et al. reported a solid volatilizable additive with a similar end-group structure of IT-4F to enhance the intermolecular interaction of small molecules in the active layer.[118,119] Likewise, the solid-additive strategy is compatible with the Y6-series. Cui et al. incorporated a valid solid additive dithieno [3,2-b:2′,3′-d]thiophene (DTT) with high crystallinity to fabricate high-performance ternary OSCs with an enhanced PCE of 18.89% and a remarkable FF of 80.6% based on PTQ10:m-BTP-PhC6:$PC_{71}BM$ blend.[119] They attributed the improved performance to the inhibition of the over-aggregation as well as the enhanced molecular packing. The critical operating principle of the solid additive is mainly attributed to the similar terminal moieties with NFAs, which can provide multiple π–π stacking pairs between end groups between the solid additive and the host NFAs. During the BHJ film formation process, the film drying kinetics and thermodynamic miscibility are believed to influence the nanostructure of crystalline and mixed regions and thus the final formation of BHJ morphology.[110,120] The different kinetics and thermodynamics of the donor and acceptor in crystallization and phase separation make BHJ morphology more unpredictable. Researchers recently found that the sequential deposition (SD) method, in which donor and acceptor solutions are separately dissolved and cast to form an active layer, can provide more processing room for optimizing two individual layers.[121–125] Li et al. performed systematic research on the morphological depiction of SD film and BHJ structure through the whole film depth with profiling depth-based morphology characterizations, giving a relative visualized depth-resolved nanomorphology. They quantitatively demonstrated that the well-defined vertical phase separation induced by the SD strategy is that—a more ordered polymer donor enriched at the cathode and a more crystallized acceptor at the anode (as illustrated in Figure 3D). It shows the excellent potential for achieving the desired vertical charge transport and surpassing the classical BHJ counterpart. More importantly, the conceptual graded-bulk heterojunction (G-BHJ) in this work is proposed to unveil the ambiguous film formation dynamics and provide a novel morphology-performance correlation enabling efficient, eco-friendly, and scalable solar cells.[92]

Since the emergence of OSCs, morphology characterization techniques have indispensably promoted the progressive fundamental morphology-performance correlations, generally involving both reciprocal space and real space characterizations, as shown in Figure 2. As the most used reciprocal space characterizations, grazing incident X-ray scattering (GIXS), mainly including GIWAXS and grazing-incidence small-angle X-ray scattering (GISAXS), can quantitatively provide molecular information, that is, the molecular crystallinity, molecular packing, and orientation ordering of active layer. For example, Liu et al. employed the GIWAXS tool to reveal that the origin of the distinct performances of PM6:Y6 OSC processed by chloroform (CF) and chlorobenzene (CB) solvents, respectively, is attributed to the different solubilities and molecular crystallinity of Y6,[101] as shown in Figure 3E. The solvent CF can induce stronger crystallinity of Y6 film, while Y6 thin film processed by CB displays low crystallinity and random orientation (as visualized by Figure 3F**)**. Thus, the CF-processed device showed higher charge carrier mobility and yielded the best PCE of 16.88%. On a larger scale, the composition distribution in the domain features, for example, domain purity and domain size (typically in the range of tens of nanometers in NFA-based thin films), can be extracted from the resonant soft X-ray scattering (R-SoXS) measurements in a highly quantitative way.[98] Wei et al. quantitatively revealed a different morphology-performance relationship in all-small molecular OSCs. Hierarchical phase separation at multiple length-scale with the coexistence of a large domain size of ∼70 nm and small domain size of ca. 10 nm in the optimal ZR1:Y6 blend benefited both charge separation and charge transport and thus increased J_{SC} and FF at the same time.[126] Considering the low composition contrast, especially in polymer-NFA OSCs due to their similar backbones, spectroscopic characterizations become increasingly significant for providing spatial

information with high chemical composition sensitivity structure, such as near-edge X-ray absorption fine structure (NEXAFS).[127] In addition to the reciprocal morphological information, microscopically, an atomic force microscopy (AFM) is popularly used to probe the film topological features like roughness and phase separation (tapping mode phase image) down to the sub-nanometers.[128] Complementary to AFM, a transmission electron microscopy (TEM) is capable of giving an average chemical element and phase composition of organic film in the bulk.[129] When the chemicals in the film have electron density contrast such as polymer versus fullerene, the computational tomography (CT) technique can be applied in TEM to visualize the 3D donor-acceptor distribution network.[130] Cross-section TEM was also adopted to show the D-A network within the cross-section. Unfortunately, entering the NFA era, the NFAs and polymer donors do not have electron microscopic contrast, and these advanced TEM approaches lose their power, and new analytical techniques need to be explored.

Other representative characterization techniques that can probe the depth-profiling of photoactive layer deserve research attention, including depth-profiling X-ray photoelectron spectroscopy (DP-XPS),[92] times-of-flight secondary ion mass spectroscopy (ToF-SIMS),[122] neutron reflectivity (NR),[131] and film-depth-dependent absorption spectroscopy.[132]

In summary, a comprehensive understanding of the complex multiscale morphology of OSC thin-film ranging from nanometers to micrometers typically depends on the complement of various technologies.

4 | STABILITY AND SCALABILITY ISSUES OF NON-FULLERENE OSCS

NFA-OSC efficiencies have undergone rapid progress over the past decades, but bearing in mind that one of the main challenges to be overcome is to close the gap between efficiency and long-term stability (operational lifetime) before moving to manufacture.[133] OSCs devices often suffer from rapid efficiency reduction in the first few hundred hours (so-called "burn-in" loss), and then they tend to reach a plateau in the following operational course upon exposure to ambient conditions, such as humidity, oxygen, light, and heat.[134,135] The ingress of environmental oxygen and moisture into the active layer, transport layers, and erosion of metal electrodes can be avoided by the firm package encapsulation of solar cells.[31] Moreover, the tolerance of active layer material to high temperature (typical operational temperature for a solar cell outdoor is 50 ∼ 60°C, and accelerated test typically uses 85°C) heavily relies on the materials' decomposition temperature.[136] Most polymer donors and NFAs possess a rather high decomposition temperature, and thus the thermal instability coming from thermal decomposition is not a significant threat. Although NFAs have better thermal stability than fullerene acceptors,[51] NFAs, unfortunately, show limited superiority in light stability,[137] which requires re-appraisement of possible degradation mechanisms. Many researchers ascribed the photo-degradation of OSCs to the chemically degraded (twisting and breakage of weak chemical bonds) structure of NFAs, particularly at the position of terminal moieties and the vinylene π-bridge linkage in both ITIC-type and Y6-type acceptors induced by high energy radiation (i.e., ultraviolet [UV]).[138–140] To address this issue, materials with novel terminals as alternatives should be preferably adopted. For instance, it has been reported that all-fused-ring electron acceptors exhibit superior light stability compared to the exocyclic double-bond NFAs.[141] Moreover, the photochemical reaction of NFAs with interfacial layers will more readily occur at the organic/inorganic interfaces when zinc oxide (ZnO) is adopted as the transporting layer.[142,143] Forrest et al. found that the inserted buffer layer (IC-SAM and C70) as a protective layer between the active layer (PCE10:BT-CIC here) and inorganic transport layers allowed much more stable inverted OSCs.[144] With the assistance of ZnO UV filter, an extrapolated T_{80} lifetime (80% of the initial PCE) exceeding 30 years of outdoor exposure was obtained, as displayed in Figure 4A. Photochemical oxidization of photoactive layer materials, especially in the presence of oxygen, is prominently mediated by the formation of highly reactive superoxide radical ions (electron transfer from NFA to oxygen), which is strongly LUMO dependent on NFA.[145] Material design of NFAs with sufficient electron affinities shallower than that of O_2 (∼3.75 eV) is a powerful way to minimize redox reactions.[146] Molecular crystallinity and packing of active layer materials is another critical concern to minimize the morphological torsion upon light-soaking. Brabec et al. reported that a $T_{80} > 10$ years via extrapolating the lifetime was achieved via fluorinating ITIC (ITIC-2F) when blended with PBDB-T, as shown in Figure 4B.[147] The unprecedented long-term stability is attributable to the well-maintained molecular packing of ITIC-2F after photo-aging compared to the initial fresh film. Apart from external stresses, it is worth noticing that in the cases without external stresses, that is, device storage in the dark, in an inert environment at room temperature, efficiency loss of NF-OSCs solar cell is still observed as a consequence of intrinsic morphology instability driven by thermodynamics factors (e.g., miscibility/comparability between donor and acceptor).[148,149] It is well accepted that the delicately optimized blend morphology of OSC film is achieved via

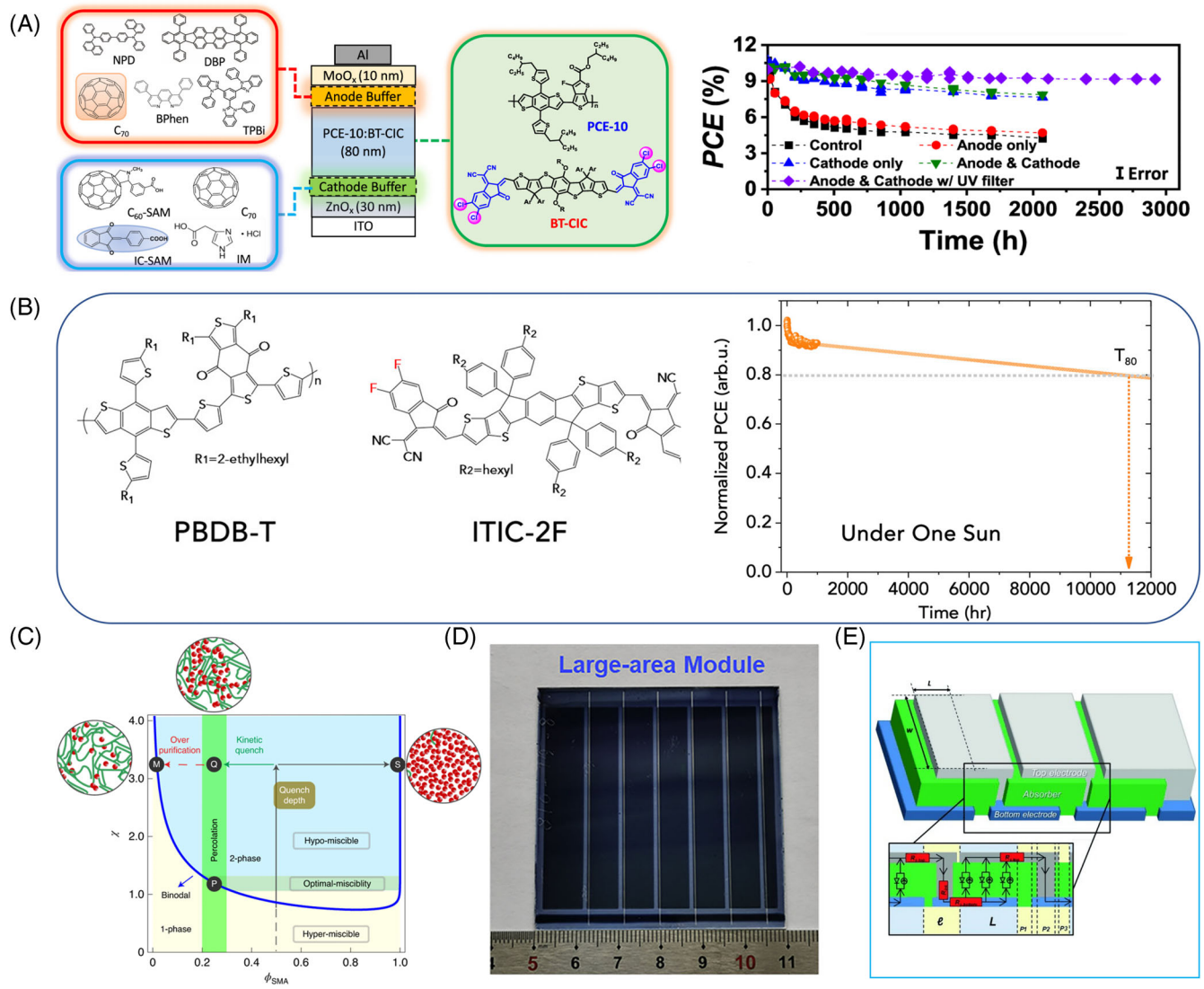

FIGURE 4 (A) Left: schematic of the device and molecular structural formulae of the PCE-10 and BT-CIC and the cathode and anode buffer materials. Right: PCE power conversion efficiency plotted versus aging time under 1 sun simulated AM1.5 G illumination for 3000 h with different device architectures (populations of 3–4 devices). The error bars indicate the 1 s.d. uncertainty of each measurement. Reproduced with permission: Copyright 2021, Springer Nature.[144] (B) The extrapolated device stability under continuous illumination in a dry nitrogen atmosphere. Reproduced with permission: Copyright 2018, Elsevier.[147] (C) The phase diagram with the binodal separating the one- and two-phase regions. Reproduced with permission: Copyright 2021, Springer Nature.[152] (D) The picture of the opaque modules based on PM6:DTY6. Reproduced with permission: Copyright 2020, Elsevier.[155] (E) Cross section of a thin-film solar module showing the key parameters for the monolithic integration: the interconnect width is represented by P2 and the patterning length is distance P1–P3 (here called here l); L represents the active cell length and w the width of the solar cell; the active area is given by $A = L{\cdot}\text{w}$. The dead area of the module, where no photo-generation occurs, corresponds to $D = l{\cdot}\text{w}$. Reproduced with permission: Copyright 2015, Wiley-VCH[156]

various processing condition optimizations, involving solvent/additive engineering, thermal, or vapor annealing, which consists of finely-mixed region and relatively separated D/A region with proper percolation thresholds for balanced charge separation and transport.[108,150] As such, the nanostructure of the active layer is kinetically trapped away from the thermodynamic equilibrium state upon solvent evaporation and is typically meta-stable, providing more significant thermodynamic driving force for demixing and morphological rearrangement via spinodal decomposition from the percolation threshold, especially in the case of the hypo-miscible (high χ) systems, which are more prone to phase segregation at room temperature and a rapid performance reduction.[151] As indicated in Figure 4C, it is thereby of significance to have optimal miscibility for OSC systems that the initial morphology is ideally close to the thermodynamic equilibrium point so that the thermodynamic driver remains small for

facilitating large assembled domains.[152] On the other hand, the substantial crystallization of NFAs is another non-negligible factor linked to the intrinsic morphological instability in OSCs.[153] Furthermore, light-soaking and heating exposure is usually susceptible to accelerating the microstructural changes (e.g., phase segregation) and thus more severe burn-in degradation in an NFA-OSC, leading to further reduction of performances, mainly FF.[154]

Another challenge in OSCs remains when upscaling small-area optimal OSCs fabricated from spin-coating method to large-area/modules devices manufactured through industrial compatible printing techniques, significant efficiency losses are typically observed at this early stage.[157] The large gap between lab to fab encourages us to highlight the governing efficiency loss mechanisms associated with the electrical and morphological aspects upon scaling. Unavoidably, series resistance (R_s) of the electrodes, especially the bottom transparent conductive electrodes (BTEs), like indium tin oxides (ITO), will increase as the solar cell area and number of cells in the module increases, leading to power losses in the large-scale device, mainly on J_{SC} and FF and no affecting the V_{OC}.[158] The transfer from small to large cells, however, involves other issues to be overcome. The thin OSC active layer (typically 80–120 nm) will encounter obstacles of film inhomogeneity and film point defects upon scaling.[159] Therefore, designing organic materials and/or morphology manipulation with high crystallinity and carrier mobility that show improved tolerance to film thickness is of great significance to produce reliable, large-area devices at an industrial scale. Ma et al. demonstrated a highly efficient slot-die coated OSC (larger area of 1 cm^2) with a PCE of 14% at the thickness of 300 nm after incorporating BTR-Cl into the control blend BTR-Cl:D18:Y6, which is ascribed to the improved crystallinity and phase purities in the finely-tuned ternary film.[42] Moreover, the varied film formation dynamics and morphological evolution between coating and printing, such as blade coating (solution shearing) and slot-die (shear impulse), set stringent requirements on modified film processing procedures, including ink concentration, solvent/additive, thermal annealing, and so forth, that can be readily adaptable for optimized spin-coating.[160] For example, the film dying rate of blend film in the blade coating process is rather slow relative to the short film drying in spin-coating driving by strong centrifugal force, often leading to the over aggregated domains. In one approach to solving this issue, a low boiling-point solvent mixture (THF/IPA) with a fast evaporation rate was rationally selected, if the solubility problem can be solved, to process PBTA-TF:IT-M OSC through blade coating.[161] The large-area 1.0 cm^2 device maintained a PCE of 10.6% via blade coating compared to 11.3% PCE with a small area of 0.04 cm^2. The in-air roll-to-roll compatible techniques for fabricating OSCs with larger sizes, for example, blade and slot-die coating, desirably require the better solubility of active layer materials in non-halogenated solvents. As discussed in the morphology, the Y-series show the distinct potential to possess superior processability via side-chain alkyl engineering on the pyrrole ring. Huang et al. replaced 2-ethylhexyl on Y6 with 2-decyltetradecyl (2-DT). The obtained molecule, DTY6, not only shows the increased solubility but also proper domain size in XY solvent without additive. The optimal device achieved an impressive PCE of 14.4% in a large-area module with an active area of 18 cm^2, as shown in Figure 4D.[155]

It should be noted that, in the cases of modules that are carefully devised in the alignment of connected subcells for providing higher voltage to drive electrical devices, the module design and processing are important.[162] For example, the interconnect part between single cells is not responsible for the current generation, which is often called dead zone, and special care should be taken to reduce the additional interconnected resistance among the single cells. The dead-zone should be reduced as much as possible to minimize so-called geometrical loss.[156] It is also of significance to rationally design module layouts, such as patterning length, patterning techniques, and active layer aspect ratio that the overall series resistance is minimized so not to influence module devices' power generation.[163,164] The existing thin-film solar technologies such as thin film amorphous silicon, CdTe, and so forth are found to be largely adoptable in OPV module. For example, the P1, P2, and P3 (Figure 4E) region design through the laser patterning process can be well accepted to reduce geometrical loss.[156]

5 | CRITICAL POTENTIAL APPLICATIONS: (SEMI) TRANSPARENT AND FLEXIBLE OSCS

Virtually any new technology enters market from critical niche applications. For OSCs, compared to traditional silicon-based solar cells, semitransparent OSCs (ST-OSCs) and flexible OSCs (F-OSCs) (as shown in Figure 5A) could be regarded as strong contenders for market entry, for example, PV windows as a new type of building-integrated photovoltaics (BIPV), on automobiles, and portable power supplies.[165] In general, the critical issue of both ST-OSCs and F-OSCs lies in innovating novel and high-performance transparent conductive

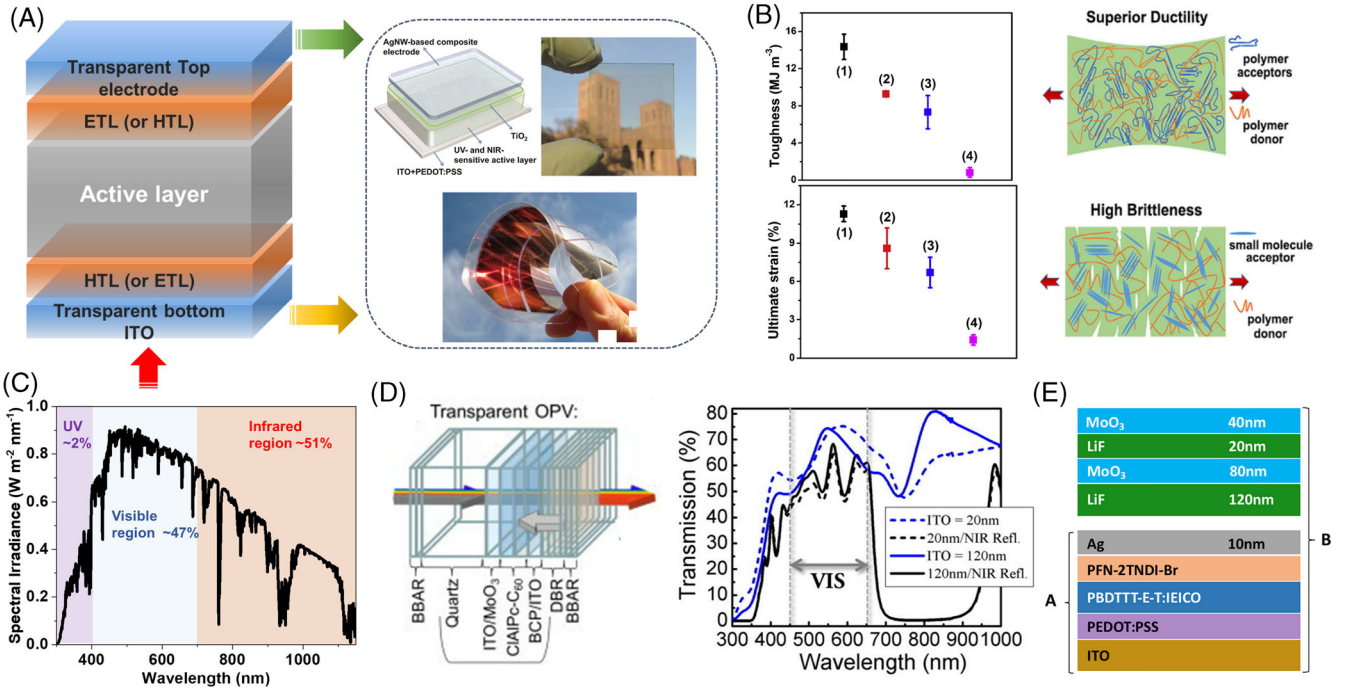

FIGURE 5 (A) The configuration of flexible and semitransparent solar cells and corresponding device images. Reproduced with permission: Copyright 2012, American Chemical Society.[169] (B) Top left: the statistical values of the toughness of active layers. Bottom left: the statistical values of the ultimate strain of active layers. Right: the schematic illustration of all polymer OSC and polymer-SMA OSC with their ductility upon bending stresses. Reproduced with permission: Copyright 2020, Elsevier.[178] (C) The solar emission spectrum with various wavelengths. (D) Schematic of the transparent photovoltaic architecture and transmission spectra of the transparent organic photovoltaic (OPV) devices for various ITO cathode thicknesses with, and without, the NIR reflector. Reproduced with permission: Copyright 2011, American Institute of Physics.[182] (E) Schematic view of the fabricated ST-OPV (device A) and ST-OPV with Bragg reflectors (device B). Reproduced with permission: Copyright 2018, Elsevier[183]

electrodes with synchronously high optical transparency and electrical conductivity. The BTEs in F-OSCs, which set additional requirements on excellent mechanical flexibility and low surface roughness, play a decisive role in determining device performances of the F-OSCs. The most used ITO electrode is mechanically brittle, which is incompatible with flexible electronic devices. It is thus urgently desirable to explore promising alternatives in F-OSCs, including conducting polymers,[166,167] metal nanowires/meshes[168,169] and graphene,[170,171] and so forth that have been extensively developed in F-OSCs. The electrodes, however, possess their respective advantages and limitations, which typically are not able to fulfill all the requirements mentioned above for high-performance F-OSCs at the same time. For example, conducting polymer PEDOT:PSS is a promising BTE due to its high mechanical tolerance to stresses but has some drawbacks, such as low conductivity and acidity, and stability.[172,173] Silver nanowires (AgNWs) become increasingly attractive electrodes with high transparency and excellent conductivity, robust mechanical ductility, stability, and scalable solution processability. However, one major problem of AgNWs as BTE that limits the PCEs in flexible OSCs is their highly rough surface morphology with random stacks, which leads to significant junction contact resistance and the leakage of current (local short-circuit).[174,175] To mitigate such issues, the composite electrode is a compromise solution that can achieve low R_s and high transmittance. As a good example, the preeminent PCE of F-OSCs based on the hybrid electrode of AgNWs/Al-doped ZnO (AZO), has reached 15.21%, PM6 as the donor material and Y6 as the acceptor material that is nearly comparable to that on rigid glass (15.78%).[176] The small gap between flexible device and rigid cell is attributed to the significantly reduced junction resistance of AgNWs through welding wire-to-wire after introducing AZO through the electrical bridge effect and capillary force effect. On the other hand, the mechanical properties of active layer material take an essential role in determining the improvement of mechanical performance of the F-OSCs. It was found that small molecules are prone to cracking when bent due to their strong tendency to aggregate in the film. Simultaneously, polymers with tangled long chains enjoy proper ductility, making them much better candidates for flexible and wearable devices.[177] Wang et al. emphasized the

higher bending durability and robust mechanical performance in all polymer OSCs, with polymerized SMA (PF2-DTSi) as a polymer acceptor.[178] The PCE maintained over 90% of the initial value after 1200 binding cycles at the bending radius of 4 mm, exceeding that of its SMA analog (IDIC), showing strong tolerance to bending stresses with a good elongation at a break of 8.6% and a large toughness value of 9.3 MJ m^{-3}, as schematically shown in Figure 5B. Polymeric additive as the third component can afford a superior mechanical robustness of the binary blend, which was demonstrated by Kim et al.[179] Likewise, Ye et al. proved that elastomer additives, which are highly viscous and insulting, can be incorporated into OSCs blends to improve the stretchability of control blends while not deteriorating the device performances.[180] Although electrical losses resulting from the highly resistive electrodes used in F-OSCs are amplified in the F-OSCs, which leads to inferior performances compared to the rigid large-area cells, it is worth noting that some exciting attempts have been progressively made toward high-performance large-area F-OSCs. Zhou et al. reported a flexible large area-based cell fabricated via the doctor-blading method with impressive PCEs of 13.1% for 6 cm^2, 12.6% for 10 cm^2 for solar cells, and 13.2% for 54 cm^2 modules, respectively, where PET/Ag grid/Ag NWs:PEI-Zn with very low Rs of 1.1 Ω sq^{-1} was adopted as the hybrid electrode.[181]

On the other hand, the narrow band structure of organic semiconductors, as well as the photoactive layer thickness of the optimal OSCs (ca. 100 nm), makes them more competitive for ST-OSCs in their potential BIPV applications.[184,185] To promote highly efficient ST-OSCs, the primary efforts should be devoted to transparent top electrodes, material screening out, and optical manipulation, in order to balance the inherent tradeoff between efficiency and average visible transmittance (AVT). As shown in Figure 5C, the NIR photons cover ~51% of the whole solar spectrum, and they are the primary source for power conversion. To achieve a high AVT, one primary route is thus to utilize NIR (and UV) responding photovoltaic materials as the photoactive layers to balance the light absorption and transmission of visible photons.[186,187] Since the state-of-the-art OSCs are mainly based on low bandgap (LBG)-NFAs with absorption up to the NIR region, and have achieved great PCEs of over 19% for opaque OSCs, the most straightforward way is to transfer the materials in opaque OSCs to ST-OSCs by reducing the thickness of top thermally evaporated metal electrodes.[4] The record OSCs typically constitute a wide bandgap (WBG) polymer donor (e.g., PM6) with the maximum absorption located at the visible regions that are blended with the acceptor in a proper weight ratio for balanced charge transport while limiting the transmittance of visible photons and thus AVT.[188] Decreasing the loading of visible absorbing donor composition in the blend is therefore the most intuitive way to minimize the visible transmittance for higher AVT. Zhang et al. gave an excellent example that they enhanced the AVT of binary blend (D18-Cl:Y6-1O) films from 30.3% to 47.3% by decreasing the D:A weight ratio from 1.1:1.6 to 0.7:1.6.[189] As a result, the corresponding optimized ST-ternary device based on D18-Cl:Y6-1O:Y6 gave a PCE of 13.02% with an AVT of 20.2%. However, the insufficient visible absorption of polymer donors in the active layer will be at the expense of device performance. Wei et al. found that reduction of donor layer thickness can be more promising in p-i-n structure in comparison with BHJ devices at the same active layer thickness. SD processed semitransparent device displayed superior average PCE of 12.91% and better AVT of 18%.[190] To further improve the efficiency of ST-OSCs at a given AVT, Li et al. applied alloyed ternary strategy with D:A_1:A_2 configuration (PM6:Y6:BTTPC) for ST-OSCs, by introducing LBG-material as the third component.[191] Consequently, the ternary opaque device exhibits an optimal PCE of 16.8%. In comparison, the semitransparent device achieved an impressive PCE of 13.1% with a well-maintained ATV of 22.4%, which effectively narrowed the tradeoff between the efficiency and transmittance. Beyond active material engineering and electrodes design, optical modulations in ST-OSCs, plays a decisive role in further minimizing the efficiency loss. The success of a near-infrared distributed Bragg reflector (DBR) in OSCs was early demonstrated by MIT group in fullerene-based OSCs, where the efficiency increased from 1.7% to the 2.4% of the opaque cell due to the extremely low transmittance in the NIR region (see Figure 5D).[182] Yip et al. introduced a DBR utilized as the transparent NIR mirror into a NFA-OSC system, which is composed of four layers of alternating materials with lithium fluoride (LiF) as low refractivity material and molybdenum trioxide (MoO_3) as high refractivity material (Figure 5E). This architecture shows higher reflectivity portion of IR region as a functional heat blocker and higher transmittance for visible light. As a result, the rationally designed ST-OSCs combined with DBR employed in active layer delivered an excellent infrared radiation rejection rate (IRR) of 80.6%, accompanied with a well maintained AVT close to 26.2%.[183]

Tandem structure is another promising strategy to construct high-performance ST-OSCs consisting of two sub-cells with NIR absorption. One such work was conducted by Yang's group.[192] They employed two LBG-OSC systems, PBDTT-FDPP-C12:$PC_{61}BM$ and PBDTT-SeDPP:$PC_{71}BM$ as the front and bottom cells, respectively. The tandem cell can achieve an improved PCE of 7.3% relative to the two sub-cells. Currently, state-of-the-art single-junction ST-OSCs exhibit the champion PCEs of 14%

with an AVT over 20% and over 15% at an AVT closing 20%.[193,194] The record light utilization efficiency (LUE) of 5.35% is achieved, and 15.10% PCE is demonstrated at 25% AVT, via novel aperiodic band-pass filter (ABPF) transparent electrode with total reflection in the NIR region (700–900 nm).[195] This has led to the belief that the tandem strategy is expected to push the efficiencies of ST-OSCs toward 17%.

6 | SUMMARY AND OUTLOOK

In summary, in this concise review article we provide a general overview of the most recent progress of NFA-OSCs, focusing on two main NFA generations (ITIC-type and Y6-type acceptors) in terms of morphology tuning of active layer and opportunities in their industrial applications, including long-term stability and scalability, hoping to foster further advances in this field. We also outline the commercial production of OSCs promoted by semitransparent and flexible OSCs. The rapid development of NFA OSCs shows opportunities to make the commercial realization of OSCs an unambiguous goal but also holds additional challenges with the following critical considerations:

1. A gap between OSCs and mature inorganic solar cells, for example, silicon, GaAs, CdTe solar cells, and hybrid perovskite solar cells still exists, mainly arising from their more considerable energy losses, typically over 0.55 eV (very few cases can suppress the value to 0.5 eV), comparing to 0.3–0.4 eV in inorganic and hybrid counterparts. Reducing energy loss via molecular structure/material design requires the in-depth investigation of chemical structure–energy loss correlation, which remains unclear. Recent studies have formulated two main rules that aim to maximize the photovoltage by reducing E_{loss}: (1) minimizing the energy offsets between donor and acceptor (i.e., charge transfer state [CT]); (2) improving the intrinsic photoluminescence quantum efficiency (PLQY) of the minimum bandgap material (typically refers to NFA), providing more efficient radiative recombination channels and low non-radiative recombination loss, which can be quantitatively determined as per EQE_{EL}.[196] Reducing energy offset is relatively intuitive to be achieved, for example, rational pairing donor and acceptor or adding the third component. Enhancing intrinsic EQE_{EL} is multi-factor correlated, including energetic and morphological properties.[82] Intrinsic chemical structure-energy loss relations remain elusive and material design, especially targeting new NFAs with higher EQE_{EL} beyond Y6, deserves key attention.
2. Morphology of active layer in both binary and ternary blends is difficult to probe due to the inherently complex local and bulk morphologies. The semicrystalline nature of organic materials and BHJ structure, included D-A interaction during film drying processes, makes the illustration of morphological features more complicated and ambiguous, posing significant challenges to the quantitative, and convincing determination of microstructure-function relations. More reliable in situ as a complement of current ex-situ morphology characterizations need more investigation to assist the insightful understanding of dynamic processes from solution to solid-state, that is, the effects on the final morphology and the OSC performances. In situ UV–vis absorption is more readily set up to detect the material aggregation dynamics of donor and acceptor; however, this is not very reliable with sometimes large variations from batch to batch, and not applicable in multicomponent systems with similar absorptions. More accurate in situ techniques with solution deposition, post-treatment, and characterization in line, such as in situ GIWAXS that could give more detailed and fast crystallinity evolution, should be more adopted, although the access of facilities is limited due to capacity and expertise. Moreover, due to the somewhat similar building blocks between polymer donors and Y6-series acceptors, low composition contrast in BHJ makes localized phase separation probing more challenging. We think the highly sensitive morphological characterization, like NEXAFS, that can be subjected to the chemical composition should be emphasized when attempting to provide insights into how to match an efficient donor–acceptor mixture, and regulate the film morphology.
3. Strengthening the NFA-OSC stability through novel design routes requires chemists to consider balancing photoelectric properties and photostability in the meantime. Y6-series acceptors with sp^2-hybridized nitrogen presumably exhibit better photo tolerance to conjugation breakage than sp^3-hybridized carbon in ITIC-type acceptors, suggesting material design is powerful in improving the intrinsic light soaking stability. For example, given that NFAs with IC terminal end-groups and vinyl typically undergo vulnerable bond cleavage, thus highly efficient and chemically stable alternatives for IC are desirably urgent. Focusing on systematic photodegradation studies especially finding out the differences between burn-in free OSC systems as previously reported[197] and OSCs with strong efficiency loss, can afford a critical guideline for identifying different degradation modes from a synthesis standpoint. Some studies indicate that non-fused NFAs have better photostability than fused

counterparts[198] and the mechanism behind it is yet to be fully elucidated, thus requiring a systematic correlation analysis. Photoactive layer morphological instability can be alleviated via device optimization, such as ternary strategy, and smart cross-linker additive, mainly aiming to inhibit aggregated NFA domains due to their strong molecular packing. Besides, sequential deposited film facilitated by inter-diffusion and aggregation dynamics has less rigid requirement for molecular miscibility, which will avoid the complex interaction between donor and acceptor during film drying processes and show great potential in improving intrinsically thermodynamic instability, in addition to clear physical picture. Furthermore, sealing materials with strong water-resistive and encapsulation methods should be exploited with the compatibility with flexible and roll-to-roll OSCs fabrication in mind. A suite of stability testing techniques with automatic measurements and software analysis in a well-defined simulated environment can benefit the long-term tracking of photovoltaic performances.

4. Unique OSC potential toward applications is in urgent need. Establishing high-performance scalable large area and flexible OSCs remains a significant concern with the following directions: developing functional and flexible electrodes, reducing efficiency loss resulting from up-scaling effects, generalizing compatible printing techniques, designing photoactive layer material ideally free from post-treatments such as high boiling point additive, or high temperature thermal annealing, as well as thickness-insensitive materials to allow >200–300 nm coating, and so forth. Transparent solar cell application is very unique for OSC over other technologies. The further boosting of TOPV figure-of-merit is very urgent to get the best balance of efficiency, AVT, color rendering index (CRI), versatility, and so forth, across all solar cell technologies. Smart transparent electrodes and it's successful scaling are no doubt critical in the next a few years to validate the feasibility of the technology.

In addition, stability of the OSCs has been a long time concern, way before perovskite PV. With encouraging results demonstrated in recently, society wide efforts using standardized reliability testing procedures, such as lifetime and mechanical stabilities in established thin film PVs are needed for effective comparison from lab-to-lab, and more importantly validate the OSC technology as whole.

ACKNOWLEDGMENTS

The authors thank the support from Research Grants Council of Hong Kong (Project Nos. 15221320, C5037-18G), Shenzhen Science and Technology Innovation Commission (Project No. JCYJ 20200109105003940), The Sir Sze-yuen Chung Endowed Professorship Fund (8-8480), and SAC5 fund provided by the Hong Kong Polytechnic University. Guangdong-Hong Kong-Macao Joint Laboratory for Photonic-Thermal-Electrical Energy Materials and Devices (GDSTC No. 2019B121205001)

CONFLICT OF INTEREST

The authors declare no conflict of interest.

ORCID

Gang Li https://orcid.org/0000-0001-8399-7771

REFERENCES

1. Li G, Zhu R, Yang Y. Polymer solar cells. *Nat Photonics*. 2012;6(3):153-161. doi:10.1038/nphoton.2012.11
2. Huang J, Li G, Yang Y. A semi-transparent plastic solar cell fabricated by a lamination process. *Adv Mater*. 2008;20(3):415-419. doi:10.1002/adma.200701101
3. Cheng P, Li G, Zhan X, Yang Y. Next-generation organic photovoltaics based on non-fullerene acceptors. *Nat Photonics*. 2018;12(3):131-142. doi:10.1038/s41566-018-0104-9
4. Li G, Chu CW, Shrotriya V, Huang J, Yang Y. Efficient inverted polymer solar cells. *Appl Phys Lett*. 2006;88(25):253503. doi:10.1063/1.2212270
5. Bae S-H, Zhao H, Hsieh Y-T, et al. Printable solar cells from advanced solution-processible materials. *Chem*. 2016;1(2):197-219. doi:10.1016/j.chempr.2016.07.010
6. Cheng Y-J, Yang S-H, Hsu C-S. Synthesis of conjugated polymers for organic solar cell applications. *Chem Rev*. 2009;109(11):5868-5923. doi:10.1021/cr900182s
7. Forrest SR. The path to ubiquitous and low-cost organic electronic appliances on plastic. *Nature*. 2004;49(6986):911-918. doi:10.1038/nature02498
8. Tang CW. Two-layer organic photovoltaic cell. *Appl Phys Lett*. 1986;48(2):183-185. doi:10.1063/1.96937
9. Sariciftci NS, Smilowitz L, Heeger AJ, Wudl F. Photoinduced electron transfer from a conducting polymer to buckminsterfullerene. *Science*. 1992;258(5087):1474-1476. doi:10.1126/science.258.5087.1474
10. Yu G, Gao J, Hummelen JC, Wudl F, Heeger AJ. Polymer photovoltaic cells: enhanced efficiencies via a network of internal donoracceptor heterojunctions. *Science*. 1995;270(5243):1789-1791. doi:10.1126/science.270.5243.1789
11. Cui Y, Xu Y, Yao H, et al. Single-junction organic photovoltaic cell with 19% efficiency. *Adv Mater*. 2021;33(41):2102420. doi:10.1002/adma.202102420
12. Zhu L, Zhang M, Xu J, et al. Single-junction organic solar cells with over 19% efficiency enabled by a refined double-fibril network morphology. *Nat Mater*. 2022;21(6):656-663. doi:10.1038/s41563-022-01244-y
13. Li C, Zhou J, Song J, et al. Non-fullerene acceptors with branched side chains and improved molecular packing to exceed 18% efficiency in organic solar cells. *Nat Energy*. 2021;6(6):605-613. doi:10.1038/s41560-021-00820-x
14. Dou L, You J, Hong Z, et al. 25th anniversary article: a decade of organic/polymeric photovoltaic research. *Adv Mater*. 2013;25(46):6642-6671. doi:10.1002/adma.201302563

15. Kim FS, Guo X, Watson MD, Jenekhe SA. High-mobility ambipolar transistors and high-gain inverters from a donor-acceptor copolymer semiconductor. *Adv Mater*. 2010;22(4):478-482. doi:10.1002/adma.200901819
16. Li G, Chang W-H, Yang Y. Low-bandgap conjugated polymers enabling solution-processable tandem solar cells. *Nat Rev Mater*. 2017;2(8):17043. doi:10.1038/natrevmats.2017.43
17. Scharber MC, Mühlbacher D, Koppe M, et al. Design rules for donors in bulk-heterojunction solar cells—towards 10% energy-conversion efficiency. *Adv Mater*. 2006;18(6):789-794. doi:10.1002/adma.200501717
18. Zhang Y, Liu D, Fong PWK, Li G. Investigation of low-bandgap nonfullerene acceptor-based polymer solar cells with very low photovoltage loss. *J Photonics Energy*. 2019;9(4):045502. doi:10.1117/1.JPE.9.045502
19. Yan C, Ma R, Cai G, et al. Reducing V_{OC} loss via structure compatible and high lowest unoccupied molecular orbital nonfullerene acceptors for over 17%-efficiency ternary organic photovoltaics. *EcoMat*. 2020;2(4):12061. doi:10.1002/eom2.12061
20. Guo X, Zhou N, Lou SJ, et al. Polymer solar cells with enhanced fill factors. *Nat Photonics*. 2013;7(10):825-833. doi:10.1038/nphoton.2013.207
21. Bartesaghi D, Perez IC, Kniepert J, et al. Competition between recombination and extraction of free charges determines the fill factor of organic solar cells. *Nat Commun*. 2015;6(1):7083. doi:10.1038/ncomms8083
22. Gasparini N, Jiao X, Heumueller T, et al. Designing ternary blend bulk heterojunction solar cells with reduced carrier recombination and a fill factor of 77%. *Nat Energy*. 2016;1(9):16118. doi:10.1038/nenergy.2016.118
23. Chen H-Y, Hou J, Zhang S, et al. Polymer solar cells with enhanced open-circuit voltage and efficiency. *Nat Photonics*. 2009;3(11):649-653. doi:10.1038/nphoton.2009.192
24. Yang Y, Chen W, Dou L, et al. High-performance multiple-donor bulk heterojunction solar cells. *Nat Photonics*. 2015;9(3):190-198. doi:10.1038/nphoton.2015.9
25. Liang Y, Xu Z, Xia J, et al. For the bright future-bulk heterojunction polymer solar cells with power conversion efficiency of 7.4%. *Adv Mater*. 2010;22(20):135-138. doi:10.1002/adma.200903528
26. Liu Y, Zhao J, Li Z, et al. Aggregation and morphology control enables multiple cases of high-efficiency polymer solar cells. *Nat Commun*. 2014;5(1):5293. doi:10.1038/ncomms6293
27. Kan B, Li M, Zhang Q, et al. A series of simple oligomer-like small molecules based on oligothiophenes for solution-processed solar cells with high efficiency. *J Am Chem Soc*. 2015;137(11):3886-3893. doi:10.1021/jacs.5b00305
28. Sun K, Xiao Z, Lu S, et al. A molecular nematic liquid crystalline material for high-performance organic photovoltaics. *Nat Commun*. 2015;6(1):6013. doi:10.1038/ncomms7013
29. Zhang G, Zhao J, Chow PCY, et al. Nonfullerene acceptor molecules for bulk heterojunction organic solar cells. *Chem Rev*. 2018;118(7):3447-3507. doi:10.1021/acs.chemrev.7b00535
30. He Y, Li Y. Fullerene derivative acceptors for high performance polymer solar cells. *Phys Chem Chem Phys*. 2011;13(6):1970-1983. doi:10.1039/C0CP01178A
31. Cheng P, Zhan X. Stability of organic solar cells: challenges and strategies. *Chem Soc Rev*. 2016;45(9):2544-2582. doi:10.1039/C5CS00593K
32. Yan C, Barlow S, Wang Z, et al. Non-fullerene acceptors for organic solar cells. *Nat Rev Mater*. 2018;3(3):18003. doi:10.1038/natrevmats.2018.3
33. Zhang J, Tan HS, Guo X, Facchetti A, Yan H. Material insights and challenges for non-fullerene organic solar cells based on small molecular acceptors. *Nat Energy*. 2018;3(9):720-731. doi:10.1038/s41560-018-0181-5
34. Li S, Ye L, Zhao W, et al. Energy-level modulation of small-molecule electron acceptors to achieve over 12% efficiency in polymer solar cells. *Adv Mater*. 2016;28(42):9423-9429. doi:10.1002/adma.201602776
35. Yao H, Chen Y, Qin Y, et al. Design and synthesis of a low band-gap small molecule acceptor for efficient polymer solar cells. *Adv Mater*. 2016;28(37):8283-8287. doi:10.1002/adma.201602642
36. Huang Y, Kramer EJ, Heeger AJ, Bazan GC. Bulk heterojunction solar cells: morphology and performance relationships. *Chem Rev*. 2014;114(14):7006-7043. doi:10.1021/cr400353v
37. Li G, Shrotriya V, Huang J, et al. High-efficiency solution processable polymer photovoltaic cells by self-organization of polymer blends. *Nat Mater*. 2005;4(11):864-868. doi:10.1038/nmat1500
38. Ma W, Yang C, Gong X, Lee K, Heeger AJ. Thermally stable, efficient polymer solar cells with nanoscale control of the interpenetrating network morphology. *Adv Funct Mater*. 2005;15(10):1617-1622. doi:10.1002/adfm.200500211
39. Zhang J, Zhang Y, Fang J, et al. Conjugated polymer-small molecule alloy leads to high efficient ternary organic solar cells. *J Am Chem Soc*. 2015;137(25):8176-8183. doi:10.1021/jacs.5b03449
40. Nian L, Kan Y, Wang H, et al. Ternary non-fullerene polymer solar cells with 13.51% efficiency and a record-high fill factor of 78.13%. *Energy Environ Sci*. 2018;11(12):3392-3399. doi:10.1039/C8EE01564C
41. Rivnay J, Mannsfeld SC, Miller CE, Salleo A, Toney MF. Quantitative determination of organic semiconductor microstructure from the molecular to device scale. *Chem Rev*. 2012;112(10):5488-5519. doi:10.1021/cr3001109
42. Zhao H, Lin B, Xue J, et al. Kinetics manipulation enables high-performance thick ternary organic solar cells via R2R compatible slot-die coating. *Adv Mater*. 2021;34(7):2105114. doi:10.1002/adma.202105114
43. Lin Y, Wang J, Zhang ZG, et al. An electron acceptor challenging fullerenes for efficient polymer solar cells. *Adv Mater*. 2015;27(7):1170-1174. doi:10.1002/adma.201404317
44. Yuan J, Zhang Y, Zhou L, et al. Single-junction organic solar cell with over 15% efficiency using fused-ring acceptor with electron-deficient core. *Joule*. 2019;3(4):1140-1151. doi:10.1016/j.joule.2019.01.004
45. Wei Q, Yuan J, Yi Y, Zhang C, Zou Y. Y6 and its derivatives: molecular design and physical mechanism. *Natl Sci Rev*. 2021;8(8):nwab121. doi:10.1093/nsr/nwab121
46. Guo Q, Guo Q, Geng Y, et al. Recent advances in PM6: Y6-based organic solar cells. *Mater Chem Front*. 2021;5(8):3257-3280. doi:10.1039/D1QM00060H
47. Huo Y, Zhang H-L, Zhan X. Nonfullerene all-small-molecule organic solar cells. *ACS Energy Lett*. 2019;4(6):1241-1250. doi:10.1021/acsenergylett.9b00528
48. Yang M, Wei W, Zhou X, Wang Z, Duan C. Non-fused ring acceptors for organic solar cells. *Energy Mater*. 2021;1(1):10008. doi:10.20517/energymater.2021.08

49. Wu B, Yin B, Duan C, Ding L. All-polymer solar cells. *J Semicond*. 2021;42(8):080301. doi:10.1088/1674-4926/42/8/080301
50. Lin Y, He Q, Zhao F, et al. A facile planar fused-ring electron acceptor for as-cast polymer solar cells with 8.71% efficiency. *J Am Chem Soc*. 2016;138(9):2973-2976. doi:10.1021/jacs.6b00853
51. Zhao W, Qian D, Zhang S, et al. Fullerene-free polymer solar cells with over 11% efficiency and excellent thermal stability. *Adv Mater*. 2016;28(23):4734-4739. doi:10.1002/adma.201600281
52. Hou J, Inganas O, Friend RH, Gao F. Organic solar cells based on non-fullerene acceptors. *Nat Mater*. 2018;17(2):119-128. doi:10.1038/nmat5063
53. Yao H, Ye L, Hou J, et al. Achieving highly efficient nonfullerene organic solar cells with improved intermolecular interaction and open-circuit voltage. *Adv Mater*. 2017;29(21):1700254. doi:10.1002/adma.201700254
54. Vandewal K, Ma Z, Bergqvist J, et al. Quantification of quantum efficiency and energy losses in low bandgap polymer: fullerene solar cells with high open-circuit voltage. *Adv Funct Mater*. 2012;22(16):3480-3490. doi:10.1002/adfm.201200608
55. Dai S, Zhao F, Zhang Q, et al. Fused nonacyclic electron acceptors for efficient polymer solar cells. *J Am Chem Soc*. 2017;139(3):1336-1343. doi:10.1021/jacs.6b12755
56. Lin Y, Zhao F, He Q, et al. High-performance electron acceptor with thienyl side chains for organic photovoltaics. *J Am Chem Soc*. 2016;138(14):4955-4961. doi:10.1021/jacs.6b02004
57. Zhao W, Li S, Yao H, et al. Molecular optimization enables over 13% efficiency in organic solar cells. *J Am Chem Soc*. 2017;139(21):7148-7151. doi:10.1021/jacs.7b02677
58. Zhang H, Yao H, Hou J, et al. Over 14% efficiency in organic solar cells enabled by chlorinated nonfullerene small-molecule acceptors. *Adv Mater*. 2018;30(28):1800613. doi:10.1002/adma.201800613
59. Yuan J, Huang T, Cheng P, et al. Enabling low voltage losses and high photocurrent in fullerene-free organic photovoltaics. *Nat Commun*. 2019;10(1):570. doi:10.1038/s41467-019-08386-9
60. Yuan J, Zou Y. The history and development of Y6. *Org Electron*. 2022;102:106436. doi:10.1016/j.orgel.2022.106436
61. Li W, Chen M, Cai J, et al. Molecular order control of nonfullerene acceptors for high-efficiency polymer solar cells. *Joule*. 2019;3(3):819-833. doi:10.1016/j.joule.2018.11.023
62. Zhang Z, Li Y, Cai G, Zhang Y, Lu X, Lin Y. Selenium heterocyclic electron acceptor with small urbach energy for as-cast high-performance organic solar cells. *J Am Chem Soc*. 2020;142(44):18741-18745. doi:10.1021/jacs.0c08557
63. Li S, Li C-Z, Shi M, Chen H. New phase for organic solar cell research: emergence of Y-series electron acceptors and their perspectives. *ACS Energy Lett*. 2020;5(5):1554-1567. doi:10.1021/acsenergylett.0c00537
64. Yao H, Ye L, Zhang H, Li S, Zhang S, Hou J. Molecular design of benzodithiophene-based organic photovoltaic materials. *Chem Rev*. 2016;116(12):7397-7457. doi:10.1021/acs.chemrev.6b00176
65. Zhang M, Guo X, Ma W, Ade H, Hou J. A large-bandgap conjugated polymer for versatile photovoltaic applications with high performance. *Adv Mater*. 2015;27(31):4655-4660. doi:10.1002/adma.201502110
66. Liu Q, Jiang Y, Jin K, et al. 18% efficiency organic solar cells. *Sci Bull*. 2020;65(4):272-275. doi:10.1016/j.scib.2020.01.001
67. Wu Y, Zheng Y, Yang H, et al. Rationally pairing photoactive materials for high-performance polymer solar cells with efficiency of 16.53%. *Sci China Chem*. 2019;63(2):265-271. doi:10.1007/s11426-019-9599-1
68. Chen H, Hu D, Yang Q, et al. All-small-molecule organic solar cells with an ordered liquid crystalline donor. *Joule*. 2019;3(12):3034-3047. doi:10.1016/j.joule.2019.09.009
69. Zhang Y, Li G. Functional third components in nonfullerene acceptor-based ternary organic solar cells. *Acc Mater Res*. 2020;1(2):158-171. doi:10.1021/accountsmr.0c00033
70. Fan B, Ying L, Zhu P, et al. All-polymer solar cells based on a conjugated polymer containing siloxane-functionalized side chains with efficiency over 10. *Adv Mater*. 2017;29(47):1703906. doi:10.1002/adma.201703906
71. Zheng N, Mahmood K, Zhong W, et al. Improving the efficiency and stability of non-fullerene polymer solar cells by using N2200 as the additive. *Nano Energy*. 2019;58:724-731. doi:10.1016/j.nanoen.2019.01.082
72. Zhang ZG, Li Y. Polymerized small-molecule acceptors for high-performance all-polymer solar cells. *Angew Chem Int Ed*. 2021;60(9):4422-4433. doi:10.1002/anie.202009666
73. Zhang ZG, Yang Y, Yao J, et al. Constructing a strongly absorbing low-bandgap polymer acceptor for high-performance all-polymer solar cells. *Angew Chem Int Ed*. 2017;56(43):13503-13507. doi:10.1002/anie.201707678
74. Jia T, Zhang J, Zhong W, et al. 14.4% efficiency all-polymer solar cell with broad absorption and low energy loss enabled by a novel polymer acceptor. *Nano Energy*. 2020;72:104718. doi:10.1016/j.nanoen.2020.104718
75. Wang W, Wu Q, Sun R, et al. Controlling molecular mass of low-band-gap polymer acceptors for high-performance all-polymer solar cells. *Joule*. 2020;4(5):1070-1086. doi:10.1016/j.joule.2020.03.019
76. Du J, Hu K, Zhang J, et al. Polymerized small molecular acceptor based all-polymer solar cells with an efficiency of 16.16% via tuning polymer blend morphology by molecular design. *Nat Commun*. 2021;12(1):5264. doi:10.1038/s41467-021-25638-9
77. Liu T, Yang T, Ma R, et al. 16% efficiency all-polymer organic solar cells enabled by a finely tuned morphology via the design of ternary blend. *Joule*. 2021;5(4):914-930. doi:10.1016/j.joule.2021.02.002
78. Sun R, Wang W, Yu H, et al. Achieving over 17% efficiency of ternary all-polymer solar cells with two well-compatible polymer acceptors. *Joule*. 2021;5(6):1548-1565. doi:10.1016/j.joule.2021.04.007
79. Luo Z, Ma R, Liu T, et al. Fine-tuning energy levels via asymmetric end groups enables polymer solar cells with efficiencies over 17%. *Joule*. 2020;4(6):1236-1247. doi:10.1016/j.joule.2020.03.023
80. Zhou K, Xian K, Ye L. Morphology control in high-efficiency all-polymer solar cells. *InfoMat*. 2022;4(4):12270. doi:10.1002/inf2.12270
81. Xie B, Zhang K, Hu Z, et al. Polymer pre-aggregation enables optimal morphology and high-performance in all-polymer solar cells. *Solar RRL*. 2019;4(3):1900385. doi:10.1002/solr.201900385
82. Xia H, Zhang Y, Deng W, et al. Novel oligomer enables green solvent processed 17.5% ternary organic solar cells: synergistic

energy loss reduction and morphology fine-tuning. *Adv Mater*. 2022;34(10):2107659. doi:10.1002/adma.202107659

83. Pang S, Wang Z, Yuan X, et al. A facile synthesized polymer featuring B-N covalent bond and small singlet-triplet gap for high-performance organic solar cells. *Angew Chem Int Ed*. 2021;60(16):8813-8817. doi:10.1002/anie.202016265
84. Yuan X, Zhao Y, Zhan T, et al. A donor polymer based on 3-cyanothiophene with superior batch-to-batch reproducibility for high-efficiency organic solar cells. *Energy Environ Sci*. 2021;14(10):5530-5540. doi:10.1039/D1EE01957K
85. Yuan X, Zhao Y, Zhang Y, et al. Achieving 16% efficiency for polythiophene organic solar cells with a cyano-substituted polythiophene. *Adv Funct Mater*. 2022;32(24):2201142. doi:10.1002/adfm.202201142
86. Yuan XY, Zhao YL, Xie DS, et al. Polythiophenes for organic solar cells with efficiency surpassing 17%. *Joule*. 2022;6(3):647-661. doi:10.1016/j.joule.2022.02.006
87. Zhao F, Wang C, Zhan X. Morphology control in organic solar cells. *Adv Energy Mater*. 2018;8(28):1703147. doi:10.1002/aenm.201703147
88. Li G, Yao Y, Yang H, Shrotriya V, Yang G, Yang Y. "Solvent annealing" effect in polymer solar cells based on poly(3-hexylthiophene) and methanofullerenes. *Adv Funct Mater*. 2007;1(10):1636-1644. doi:10.1002/adfm.200600624
89. Karki A, Vollbrecht J, Gillett AJ, et al. The role of bulk and interfacial morphology in charge generation, recombination, and extraction in non-fullerene acceptor organic solar cells. *Energy Environ Sci*. 2020;13(10):3679-3692. doi:10.1039/D0EE01896A
90. Gao J, Chen W, Dou L, et al. Elucidating double aggregation mechanisms in the morphology optimization of diketopyrrolopyrrole-based narrow bandgap polymer solar cells. *Adv Mater*. 2014;26(19):3142-3147. doi:10.1002/adma.201305645
91. Yao E-P, Chen C-C, Gao J, et al. The study of solvent additive effects in efficient polymer photovoltaics via impedance spectroscopy. *Sol Energy Mater Sol Cells*. 2014;130:20-26. doi:10.1016/j.solmat.2014.05.049
92. Zhang Y, Liu K, Huang J, et al. Graded bulk-heterojunction enables 17% binary organic solar cells via nonhalogenated open air coating. *Nat Commun*. 2021;12(1):4815. doi:10.1038/s41467-021-25148-8
93. Zhao J, Li Y, Yang G, et al. Efficient organic solar cells processed from hydrocarbon solvents. *Nat Energy*. 2016;1(2):15027. doi:10.1038/nenergy.2015.27
94. Yao Y, Hou J, Xu Z, Li G, Yang Y. Effects of solvent mixtures on the nanoscale phase separation in polymer solar cells. *Adv Funct Mater*. 2008;18(12):1783-1789. doi:10.1002/adfm.200701459
95. Lv J, Tang H, Huang J, et al. Additive-induced miscibility regulation and hierarchical morphology enable 17.5% binary organic solar cells. *Energy Environ Sci*. 2021;14(5):3044-3052. doi:10.1039/D0EE04012F
96. Muller BP. The active layer morphology of organic solar cells probed with grazing incidence scattering techniques. *Adv Mater*. 2014;26(46):7692-7709. doi:10.1002/adma.201304187
97. Luginbuhl BR, Raval P, Pawlak T, et al. Resolving atomic-scale interactions in non-fullerene acceptor organic solar cells with solid-state NMR spectroscopy, crystallographic modelling, and molecular dynamics simulations. *Adv Mater*. 2021;34(6):2105943. doi:10.1002/adma.202105943
98. Jiao X, Ye L, Ade H. Quantitative morphology–performance correlations in organic solar cells: insights from soft X-ray scattering. *Adv Energy Mater*. 2017;7(18):1700084. doi:10.1002/aenm.201700084
99. Zhang Y, Liu D, Lau TK, et al. A novel wide-bandgap polymer with deep ionization potential enables exceeding 16% efficiency in ternary nonfullerene polymer solar cells. *Adv Funct Mater*. 2020;30(27):1910466. doi:10.1002/adfm.201910466
100. Lai H, Zhao Q, Chen Z, et al. Trifluoromethylation enables a 3D interpenetrated low-band-gap acceptor for efficient organic solar cells. *Joule*. 2020;4(3):688-700. doi:10.1016/j.joule.2020.02.004
101. Zhu L, Zhang M, Zhou G, et al. Efficient organic solar cell with 16.88% efficiency enabled by refined acceptor crystallization and morphology with improved charge transfer and transport properties. *Adv Energy Mater*. 2020;10(8):1904234. doi:10.1002/aenm.201904234
102. Kupgan G, Chen XK, Brédas JL. Molecular packing of non-fullerene acceptors for organic solar cells: distinctive local morphology in Y6 vs. ITIC derivatives. *Mater Today Adv*. 2021;11:100154. doi:10.1016/j.mtadv.2021.100154
103. Lin F, Jiang K, Kaminsky W, Zhu Z, Jen AK. A non-fullerene acceptor with enhanced intermolecular pi-core interaction for high-performance organic solar cells. *J Am Chem Soc*. 2020;142(36):15246-15251. doi:10.1021/jacs.0c07083
104. Zhang G, Chen XK, Xiao J, et al. Delocalization of exciton and electron wavefunction in non-fullerene acceptor molecules enables efficient organic solar cells. *Nat Commun*. 2020;11(1):3943. doi:10.1038/s41467-020-17867-1
105. Hong L, Yao H, Wu Z, et al. Eco-compatible solvent-processed organic photovoltaic cells with over 16% efficiency. *Adv Mater*. 2019;31(39):e1903441. doi:10.1002/adma.201903441
106. Cui Y, Yao H, Zhang J, et al. Single-junction organic photovoltaic cells with approaching 18% efficiency. *Adv Mater*. 2020;32(19):1908205. doi:10.1002/adma.201908205
107. Chen H, Zhang R, Chen X, et al. A guest-assisted molecular-organization approach for >17% efficiency organic solar cells using environmentally friendly solvents. *Nat Energy*. 2021;6(11):1045-1053. doi:10.1038/s41560-021-00923-5
108. Ye L, Hu H, Ghasemi M, et al. Quantitative relations between interaction parameter, miscibility and function in organic solar cells. *Nat Mater*. 2018;17(3):253-260. doi:10.1038/s41563-017-0005-1
109. Xu X, Li Y, Peng Q. Recent advances in morphology optimizations towards highly efficient ternary organic solar cells. *Nano Select*. 2020;1(1):30-58. doi:10.1002/nano.202000012
110. Naveed HB, Ma W. Miscibility-driven optimization of nanostructures in ternary organic solar cells using non-fullerene acceptors. *Joule*. 2018;2(4):621-641. doi:10.1016/j.joule.2018.02.010
111. Xu X, Li Y, Peng Q. Ternary blend organic solar cells: understanding the morphology from recent progress. *Adv Mater*. 2021;2107476. doi:10.1002/adma.202107476
112. Tang H, Lv J, Liu K, et al. Self-assembly enables simple structure organic photovoltaics via green-solvent and open-air-printing: closing the lab-to-fab gap. *Mater Today*. 2022;55:46-55. doi:10.1016/j.mattod.2022.04.005
113. Ye L, Li S, Liu X, et al. Quenching to the percolation threshold in organic solar cells. *Joule*. 2019;3(2):443-458. doi:10.1016/j.joule.2018.11.006

114. Wang Z, Peng Z, Xiao Z, et al. Thermodynamic properties and molecular packing explain performance and processing procedures of three D18:NFA organic solar cells. *Adv Mater*. 2020; 32(49):2005386. doi:10.1002/adma.202005386
115. Tang H, Chen H, Yan C, et al. Delicate morphology control triggers 14.7% efficiency all-small-molecule organic solar cells. *Adv Energy Mater*. 2020;10(27):2001076. doi:10.1002/aenm.202001076
116. Zhan L, Li S, Lau T-K, et al. Over 17% efficiency ternary organic solar cells enabled by two non-fullerene acceptors working in alloy-like model. *Energy Environ Sci*. 2020;13(2): 635-645. doi:10.1039/C9EE03710A
117. Bi P, Zhang S, Chen Z, et al. Reduced non-radiative charge recombination enables organic photovoltaic cell approaching 19% efficiency. *Joule*. 2021;5(9):2408-2419. doi:10.1016/j.joule.2021.06.020
118. Yu R, Yao H, Hong L, et al. Design and application of volatilizable solid additives in non-fullerene organic solar cells. *Nat Commun*. 2018;9(1):4645. doi:10.1038/s41467-018-07017-z
119. Bao S, Yang H, Fan H, et al. Volatilizable solid additive-assisted treatment enables organic solar cells with efficiency over 18.8% and fill factor exceeding 80%. *Adv Mater*. 2021;33: 2105301. doi:10.1002/adma.202105301
120. Zhu L, Zhong W, Qiu C, et al. Aggregation-induced multilength scaled morphology enabling 11.76% efficiency in all-polymer solar cells using printing fabrication. *Adv Mater*. 2019;31(41):e1902899. doi:10.1002/adma.201902899
121. Aguirre JC, Hawks SA, Ferreira AS, et al. Sequential processing for organic photovoltaics: design rules for morphology control by tailored semi-orthogonal solvent blends. *Adv Energy Mater*. 2015;5(11):1402020. doi:10.1002/aenm.201402020
122. Zhan L, Li S, Xia X, et al. Layer-by-layer processed ternary organic photovoltaics with efficiency over 18. *Adv Mater*. 2021;33(12):2007231. doi:10.1002/adma.202007231
123. Kumar A, Li G, Hong Z, Yang Y. High efficiency polymer solar cells with vertically modulated nanoscale morphology. *Nanotechnology*. 2009;20(16):165202. doi:10.1088/0957-4484/20/16/165202
124. Lee DH, Michael YY, You J, Richard E, Li G. Immiscible solvents enabled nanostructure formation for efficient polymer photovoltaic cells. *Nanotechnology*. 2014;25(29):295401. doi:10.1088/0957-4484/25/29/295401
125. Wang DH, Moon JS, Seifter J, et al. Sequential processing: control of nanomorphology in bulk heterojunction solar cells. *Nano Lett*. 2011;11(8):3163-3168. doi:10.1021/nl202320r
126. Zhou R, Jiang Z, Yang C, et al. All-small-molecule organic solar cells with over 14% efficiency by optimizing hierarchical morphologies. *Nat Commun*. 2019;10(1):5393. doi:10.1038/s41467-019-13292-1
127. Ade H, Stoll H. Near-edge X-ray absorption fine-structure microscopy of organic and magnetic materials. *Nat Mater*. 2009;8(4):281-290. doi:10.1038/nmat2399
128. Giessibl FJ. Advances in atomic force microscopy. *Rev Mod Phys*. 2003;75(3):949-983. doi:10.1103/RevModPhys.75.949
129. Varela M, Lupini AR, Van Benthem K, et al. Materials characterization in the aberration-corrected scanning transmission electron microscope. *Annu Rev Mater*. 2005;35(1):539-569. doi:10.1146/annurev.matsci.35.102103.090513
130. Yang X, Loos J. Toward high-performance polymer solar cells: the importance of morphology control. *Macromolecules*. 2007; 40(5):1353-1362. doi:10.1021/ma0618732
131. Li Q, Wang L-M, Liu S, et al. Vertical composition distribution and crystallinity regulations enable high-performance polymer solar cells with >17% efficiency. *ACS Energy Lett*. 2020; 5(11):3637-3646. doi:10.1021/acsenergylett.0c01927
132. Weng K, Ye L, Zhu L. Optimized active layer morphology toward efficient and polymer batch insensitive organic solar cells. *Nat Commun*. 2020;11(1):2855. doi:10.1038/s41467-020-16621-x
133. Brabec CJ. Organic photovoltaics: technology and market. *Sol Energy Mater Sol Cells*. 2004;83(2–3):273-292. doi:10.1016/j.solmat.2004.02.030
134. Li N, Perea JD, Kassar T, et al. Abnormal strong burn-in degradation of highly efficient polymer solar cells caused by spinodal donor-acceptor demixing. *Nat Commun*. 2017;8(1): 14541. doi:10.1038/ncomms14541
135. Baran D, Ashraf RS, Hanifi DA, et al. Reducing the efficiency-stability-cost gap of organic photovoltaics with highly efficient and stable small molecule acceptor ternary solar cells. *Nat Mater*. 2017;16(3):363-369. doi:10.1038/nmat4797
136. Duan L, Uddin A. Progress in stability of organic solar cells. *Adv Sci*. 2020;7(11):1903259. doi:10.1002/advs.201903259
137. Park S, Son HJ. Intrinsic photo-degradation and mechanism of polymer solar cells: the crucial role of non-fullerene acceptors. *J Mater Chem A*. 2019;7(45):25830-25837. doi:10.1039/C9TA07417A
138. Guo J, Wu Y, Sun R, et al. Suppressing photo-oxidation of non-fullerene acceptors and their blends in organic solar cells by exploring material design and employing friendly stabilizers. *J Mater Chem A*. 2019;7(43):25088-25101. doi:10.1039/C9TA09961A
139. Zhao Y, Wu Z, Liu X, Zhong Z, Zhu R, Yu J. Revealing the photo-degradation mechanism of PM6:Y6 based high-efficiency organic solar cells. *J Mater Chem C*. 2021;9(39): 13972-13980. doi:10.1039/D1TC03655F
140. Zhu X, Liu S, Yue Q, Liu W, Sun S, Xu S. Design of all-fused-ring electron acceptors with high thermal, chemical, and photochemical stability for organic photovoltaics. *CCS Chem*. 2021;3(6):1070-1080. doi:10.31635/ccschem.021.202100956
141. Liu W, Xu S, Lai H, Liu W, He F, Zhu X. Near-infrared all-fused-ring nonfullerene acceptors achieving an optimal efficiency-cost-stability balance in organic solar cells. *CCS Chem*. 2022;1-15. doi:10.31635/ccschem.022.202201963
142. Jiang Y, Sun L, Jiang F, et al. Photocatalytic effect of ZnO on the stability of nonfullerene acceptors and its mitigation by SnO_2 for nonfullerene organic solar cells. *Mater Horiz*. 2019; 6(7):1438-1443. doi:10.1039/C9MH00379G
143. Liu B, Han Y, Li Z, et al. Visible light–induced degradation of inverted polymer: nonfullerene acceptor solar cells: initiated by the light absorption of ZnO layer. *Sol RRL*. 2021;5(1): 2000638. doi:10.1002/solr.202000638
144. Li Y, Huang X, Ding K, et al. Non-fullerene acceptor organic photovoltaics with intrinsic operational lifetimes over 30 years. *Nat Commun*. 2021;12(1):5419. doi:10.1038/s41467-021-25718-w
145. Gasparini N, Salleo A, McCulloch I, Baran D. The role of the third component in ternary organic solar cells. *Nat Rev Mater*. 2019;4(4):229-242. doi:10.1038/s41578-019-0093-4

146. Leeuw DM, Simenon MMJ, Brown AR, Einerhand REF. Stability of n-type doped conducting polymers and consequences for polymeric microelectronic devices. *Synth Met*. 1997;87(1):53-59. doi:10.1016/S0379-6779(97)80097-5
147. Du X, Heumueller T, Gruber W, et al. Efficient polymer solar cells based on non-fullerene acceptors with potential device lifetime approaching 10 years. *Joule*. 2019;3(1):215-226. doi:10.1016/j.joule.2018.09.001
148. Ghasemi M, Hu H, Peng Z, et al. Delineation of thermodynamic and kinetic factors that control stability in non-fullerene organic solar cells. *Joule*. 2019;3(5):1328-1348. doi:10.1016/j.joule.2019.03.020
149. Hu H, Ghasemi M, Peng Z, et al. The role of demixing and crystallization kinetics on the stability of non-fullerene organic solar cells. *Adv Mater*. 2020;32(49):2005348. doi:10.1002/adma.202005348
150. Burlingame Q, Ball M, Loo Y-L. It's time to focus on organic solar cell stability. *Nat Energy*. 2020;5(12):947-949. doi:10.1038/s41560-020-00732-2
151. Du X, Heumueller T, Gruber W, et al. Unraveling the microstructure-related device stability for polymer solar cells based on nonfullerene small-molecular acceptors. *Adv Mater*. 2020;32(16):1908305. doi:10.1002/adma.201908305
152. Ghasemi M, Balar N, Peng Z, et al. A molecular interaction-diffusion framework for predicting organic solar cell stability. *Nat Mater*. 2021;20(4):525-532. doi:10.1038/s41563-020-00872-6
153. Zhu Y, Gadisa A, Peng Z, et al. Rational strategy to stabilize an unstable high-efficiency binary nonfullerene organic solar cells with a third component. *Adv Energy Mater*. 2019;9(20):1900376. doi:10.1002/aenm.201900376
154. Burlingame Q, Song B, Ciammaruchi L, et al. Reliability of small molecule organic photovoltaics with electron-filtering compound buffer layers. *Adv Energy Mater*. 2016;6(21):1601094. doi:10.1002/aenm.201601094
155. Dong S, Jia T, Zhang K, Jing J, Huang F. Single-component non-halogen solvent-processed high-performance organic solar cell module with efficiency over 14%. *Joule*. 2020;4(9):2004-2016. doi:10.1016/j.joule.2020.07.028
156. Lucera L, Kubis P, Fecher FW, et al. Guidelines for closing the efficiency gap between hero solar cells and roll-to-roll printed modules. *Energy Technol*. 2015;3(4):373-384. doi:10.1002/ente.201402192
157. Xiao Y, Zuo C, Zhong JX, Wu WQ, Shen L, Ding L. Large-area blade-coated solar cells: advances and perspectives. *Adv Energy Mater*. 2021;11(21):2100378. doi:10.1002/aenm.202100378
158. Choi S, Potscavage WJ, Kippelen B. Area-scaling of organic solar cells. *J Appl Phys*. 2009;106(5):054507. doi:10.1063/1.3211850
159. Strohm S, Machui F, Langner S, et al. P3HT: non-fullerene acceptor based large area, semi-transparent PV modules with power conversion efficiencies of 5%, processed by industrially scalable methods. *Energy Environ Sci*. 2018;11(8):2225-2234. doi:10.1039/C8EE01150H
160. Hong L, Yao H, Cui Y, Ge Z, Hou J. Recent advances in high-efficiency organic solar cells fabricated by eco-compatible solvents at relatively large-area scale. *APL Mater*. 2020;8(12):120901. doi:10.1063/5.0027948
161. Zhao W, Zhang S, Zhang Y, et al. Environmentally friendly solvent-processed organic solar cells that are highly efficient and adaptable for the blade-coating method. *Adv Mater*. 2018;30(4):1704837. doi:10.1002/adma.201704837
162. Angmo D, Hösel M, Krebs FC. All solution processing of ITO-free organic solar cell modules directly on barrier foil. *Sol Energy Mater Sol Cells*. 2012;107:329-336. doi:10.1016/j.solmat.2012.07.004
163. Wang G, Adil MA, Zhang J, Wei Z. Large-area organic solar cells: material requirements, modular designs, and printing methods. *Adv Mater*. 2019;31(45):1805089. doi:10.1002/adma.201805089
164. Riede M, Spoltore D, Leo K. Organic solar cells—the path to commercial success. *Adv Energy Mater*. 2020;11(1):2002653. doi:10.1002/aenm.202002653
165. Zuo L, Zhang S, Li H, Chen H. Toward highly efficient large-area ITO-free organic solar cells with a conductance-gradient transparent electrode. *Adv Mater*. 2015;27(43):6983-6969. doi:10.1002/adma.201502827
166. Zhang F, Johansson M, Andersson MR, Hummelen Jan C, Inganäs O. Polymer photovoltaic cells with conducting polymer anodes. *Adv Mater*. 2002;14(9):662-665.
167. Ouyang J, Chu CW, Chen FC, Xu Q, Yang Y. High-conductivity poly(3,4-ethylenedioxythiophene):poly(styrene sulfonate) film and its application in polymer optoelectronic devices. *Adv Funct Mater*. 2005;15(2):203-208. doi:10.1002/adfm.200400016
168. Wang H, Tang H, Liang J, Chen Y. Dynamic agitation-induced centrifugal purification of nanowires enabling transparent electrodes with 99.2% transmittance. *Adv Funct Mater*. 2018;28(45):1804479. doi:10.1002/adfm.201804479
169. Chen C-C, Dou L, Zhu R, et al. Visibly transparent polymer solar cells produced by solution processing. *ACS Nano*. 2012;6(8):7185-7190. doi:10.1021/nn3029327
170. Koo D, Jung S, Seo J, et al. Flexible organic solar cells over 15% efficiency with polyimide-integrated graphene electrodes. *Joule*. 2020;4(5):1021-1034. doi:10.1016/j.joule.2020.02.012
171. Liu Z, Li J, Yan F. Package-free flexible organic solar cells with graphene top electrodes. *Adv Mater*. 2013;25(31):4296-4301. doi:10.1002/adma.201205337
172. Huang J, Ren Z, Zhang Y, et al. Stretchable ITO-free organic solar cells with intrinsic anti-reflection substrate for high-efficiency outdoor and indoor energy harvesting. *Adv Funct Mater*. 2021;31(16):2010172. doi:10.1002/adfm.202010172
173. Kim YH, Sachse C, Machala ML, May C, Müller ML, Leo K. Highly conductive PEDOT:PSS electrode with optimized solvent and thermal post-treatment for ITO-free organic solar cells. *Adv Funct Mater*. 2011;21(6):1076-1081. doi:10.1002/adfm.201002290
174. Zeng G, Chen W, Chen X, et al. Realizing 17.5% efficiency flexible organic solar cells via atomic-level chemical welding of silver nanowire electrodes. *J Am Chem Soc*. 2022;144(19):8658-8668. doi:10.1021/jacs.2c01503
175. Yang Y, Xu B, Hou J. Solution-processed silver nanowire as flexible transparent electrodes in organic solar cells. *Chin J Chem*. 2021;39(8):2315-2329. doi:10.1002/cjoc.202000696
176. Chen X, Xu G, Zeng G, et al. Realizing ultrahigh mechanical flexibility and >15% efficiency of flexible organic solar cells via a "welding" flexible transparent electrode. *Adv Mater*. 2020;32(14):1908478. doi:10.1002/adma.201908478

177. Ma R, Yu J, Liu T, et al. All-polymer solar cells with over 16% efficiency and enhanced stability enabled by compatible solvent and polymer additives. *Aggregate*. 2021;58(3):e58. doi:10.1002/agt2.58
178. Fan Q, Su W, Chen S, et al. Mechanically robust all-polymer solar cells from narrow band gap acceptors with hetero-bridging atoms. *Joule*. 2020;4(3):658-672. doi:10.1016/j.joule.2020.01.014
179. Lee JW, Ma BS, Kim HJ, Kim TS, Kim BJ. High-molecular-weight electroactive polymer additives for simultaneous enhancement of photovoltaic efficiency and mechanical robustness in high-performance polymer solar cells. *J Am Chem Soc Au*. 2021;1(5):612-622. doi:10.1021/jacsau.1c00064
180. Peng Z, Xian K, Cui Y, et al. Thermoplastic elastomer tunes phase structure and promotes stretchability of high-efficiency organic solar cells. *Adv Mater*. 2021;33(49):2106732. doi:10.1002/adma.202106732
181. Qin F, Sun L, Chen H, et al. 54 cm^2 large-area flexible organic solar modules with efficiency above 13. *Adv Mater*. 2021;33(39):2103017. doi:10.1002/adma.202103017
182. Lunt RR, Bulovic V. Transparent, near-infrared organic photovoltaic solar cells for window and energy-scavenging applications. *Appl Phys Lett*. 2011;98(11):113305. doi:10.1063/1.3567516
183. Sun C, Xia R, Shi H, et al. Heat-insulating multifunctional semitransparent polymer solar cells. *Joule*. 2018;2(9):1816-1826. doi:10.1016/j.joule.2018.06.006
184. Chang S-Y, Cheng P, Li G, Yang Y. Transparent polymer photovoltaics for solar energy harvesting and beyond. *Joule*. 2018;2(6):1039-1054. doi:10.1016/j.joule.2018.04.005
185. Cheng P, Wang HC, Zhu Y, et al. Transparent hole-transporting frameworks: a unique strategy to design high-performance semitransparent organic photovoltaics. *Adv Mater*. 2020;32(39):2003891. doi:10.1002/adma.202003891
186. Wang W, Yan C, Lau TK, et al. Fused hexacyclic nonfullerene acceptor with strong near-infrared absorption for semitransparent organic solar cells with 9.77% efficiency. *Adv Mater*. 2017;29(31):1701308. doi:10.1002/adma.201701308
187. Dai S, Zhan X. Nonfullerene acceptors for semitransparent organic solar cells. *Adv Energy Mater*. 2018;8(21):1800002. doi:10.1002/aenm.201800002
188. Hu Z, Wang Z, An Q, Zhang F. Semitransparent polymer solar cells with 12.37% efficiency and 18.6% average visible transmittance. *Sci Bull*. 2020;65(2):131-137. doi:10.1016/j.scib.2019.09.016
189. Hu Z, Wang J, Ma X, et al. Semitransparent organic solar cells exhibiting 13.02% efficiency and 20.2% average visible transmittance. *J Mater Chem A*. 2021;9(11):6797-6804. doi:10.1039/D1TA01135A
190. Wang HC, Cheng P, Tan S, et al. Sequential deposition of donor and acceptor provides high-performance semitransparent organic photovoltaics having a pseudo p–i–n active layer structure. *Adv Energy Mater*. 2021;11(13):2003576. doi:10.1002/aenm.202003576
191. Wang D, Qin R, Zhou G, et al. High-performance semitransparent organic solar cells with excellent infrared reflection and see-through functions. *Adv Mater*. 2020;32(32):2001621. doi:10.1002/adma.202001621
192. Chen C-C, Dou L, Gao J, Chang W-H, Li G, Yang Y. High-performance semi-transparent polymer solar cells possessing tandem structures. *Energ Environ Sci*. 2013;6(9):2714-2720. doi:10.1039/c3ee40860d
193. Liu W, Sun S, Zhou L, et al. Design of near-infrared nonfullerene acceptor with ultralow nonradiative voltage loss for high-performance semitransparent ternary organic solar cells. *Angew Chem Int Ed Engl*. 2022;61(19):e202116111. doi:10.1002/anie.202116111
194. Jing J, Dong S, Zhang K, et al. Semitransparent organic solar cells with efficiency surpassing 15%. *Adv Energy Mater*. 2022;12(20):2200453. doi:10.1002/aenm.202200453
195. Liu X, Zhong ZP, Zhu RH, Yu JS, Li G. Aperiodic band-pass electrode enables record-performance transparent organic photovoltaics. *Joule*. 2022;6(8):1918-1930. doi:10.1016/j.joule.2022.06.009
196. Qian D, Zheng Z, Yao H, et al. Design rules for minimizing voltage losses in high-efficiency organic solar cells. *Nat Mater*. 2018;17(8):703-709. doi:10.1038/s41563-018-0128-z
197. Gasparini N, Salvador M, Strohm S, et al. Burn-in free nonfullerene-based organic solar cells. *Adv Energy Mater*. 2017;7(19):1700770. doi:10.1002/aenm.201700770
198. Yu ZP, Liu ZX, Chen FX, et al. Simple non-fused electron acceptors for efficient and stable organic solar cells. *Nat Commun*. 2019;10(1):2152. doi:10.1038/s41467-019-10098-z

AUTHOR BIOGRAPHIES

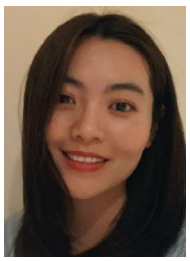

Ying Zhang obtained her M.Sc. degree from the Hong Kong University of Science and Technology. She is currently working as a postdoctoral in the Department of Electronic and Information Engineering at the Hong Kong Polytechnic University in Prof. Gang Li's group. Her primary research focuses on the device engineering of high-performance organic solar cells with novel nanostructures and understanding the device physics.

Gang Li is Sir Sze-Yuen Chung Endowed Professor in Renewable Energy in the Department of Electronic and Information Engineering, Associate Director of Research Institute of Smart Energy (RISE) in the Hong Kong Polytechnic University. He obtained his B.Sc. degree in Space Physics from Wuhan University (China), M.Sc. in Electrical Engineering, and Ph. D. in Condensed Matter Physics from Iowa State

University, respectively. His research interests are materials, device engineering, and device physics in organic semiconductors, and hybrid perovskite semiconductors, focusing on energy applications. He was a postdoc, Research Professor at UCLA, and VP of Solarmer Energy Inc. before coming to Hong Kong in 2016. He has been among Thomson Reuters/Clarivate Analytics Highly Cited Researchers since 2014. He has published ~200 papers, with over 70 000 citations and H-index of 78 (Google Scholar). He is Fellow of Royal Society of Chemistry (RSC), The International Society for Optics and Photonic (SPIE), and Optica (OSA).

How to cite this article: Zhang Y, Lang Y, Li G. Recent advances of non-fullerene organic solar cells: From materials and morphology to devices and applications. *EcoMat*. 2023;5(1):e12281. doi:10.1002/eom2.12281